University of Tartu

Faculty of Science and Technology

Institute of Ecology and Earth Sciences

Department of Geology

Bachelor's thesis in geology

Dating zircons from Francevillian Basin by laser-ablation inductively coupled plasma mass-spectrometry

Carmel Kuusk

Supervisors: Kalle Kirsimäe

Päärn Paiste

Allowed for defence:

Supervisors:

Tartu 2021

Dating zircons from Francevillian Basin by laser-ablation inductively coupled plasma mass-spectrometry

The aim of this bachelor's thesis was to measure the U-Pb ages of the zircon samples from Francevillian Basin in Gabon using laser-ablation inductively coupled plasma mass-spectrometry (LA-ICP-MS).

Three samples were from tuff-like layers from an outcrop of Francevillian FB formation, and two samples were from K-bentonites from Francevillian FD formation intersected in Doume drillcore. As a result, zircon grains from FB formation yielded U-Pb ages over 2800 Ma suggesting that these zircons are inherited from the crystalline basement of the basin. Zircon grains from FD formation did not provide very reliable data. Only one signal was considered as reliable, and this signal yielded Pb-Pb age at 2082 ± 19 Ma.

Keywords: U-Pb dating, LA-ICP-MS, zircon

CERCS: P420 Petrology, mineralogy, geochemistry

Franceville'i settebasseinist pärinevate tsirkoonide dateerimine laser-ablatsiooni induktiivsidestatud plasma massispektromeetria meetodil

Bakalaureusetöö eesmärgiks oli määrata laser-ablatsiooni induktiivsidestatud plasma massispektromeetria (LA-ICP-MS) meetodil Gabonist, Franceville'i settebasseinist kogutud tsirkoonidele U-Pb vanused.

Kolm proovi pärinesid tuffilaadsetest kihtidest Franceville'i settebasseini FB kihistu paljandproovidest. Kaks proovi pärinesid K-bentoniitidi kihist Franceville'i settebasseini FD kihistust Doume puursüdamikus. Töö tulemusena saadi FB kihistust pärit tsirkooniterade keskmisteks vanusteks rohkem kui 2800 Ma. Sellest võib järeldada, et tsirkoonid on settesse sisse kantud basseini kristalsetest aluskorra kivimitest. FD kihistust pärinevatest tsirkoonidest mõõdetud signaalid ei olnud väga usaldusväärsed. Saadi vaid üks vanus, mis hinnati usaldusväärseks ning see andis tsirkoonitera Pb-Pb vanuseks 2082 ± 19 Ma.

Märksõnad: U-Pb dateerimine, LA-ICP-MS, tsirkoon

CERCS: P420 Petroloogia, mineraloogia, geokeemia

Content

Introduction

One of the paramount events in the early development of the Earth system was the shift from anoxic to oxic surface environments at Archean to Proterozoic transition (Holland, 2006; Lyons *et al*., 2014). This change triggered progressive modification nearly of all biogeochemical cycles and provided necessary environmental conditions for development of modern life.

The rise of oxygen levels in atmosphere between 2426 to 2460 Ma (Gumsley *et al*., 2017) induced the shut-down of mass-independent fractionation (MIF) of sulphur. Which is preserved in sedimentary records and is interpreted as representing the timing of the Great Oxidation Event (GOE) (Farquhar *et al*., 2000; Luo *et al*., 2016). As an evidence of following major disturbances in (bio-)chemical cycles caused by GOE are the largest-magnitude perturbation of the carbon cycle – the Lomagundi-Jatuli Event (LJE), that occurred between 2.2-2.06 Ga (Karhu and Holland, 1996) in parallel to build-up of a sizable sulphate marine reservoir (Blättler *et al*., 2018); the ca. 2 Ga Shunga Event – a large-scale accumulation of organic-rich sediments (Melezhik *et al*., 2012); and the appearance of first phosphatic sediments (Lepland *et al*., 2013).

Timing and tempos of GOE and associated changes are still largely debated (Poulton *et al*., 2021; Martin *et al*., 2013; Gumsley *et al*., 2017). Though the evidence for these drastic geological processes are found globally in metasedimentary rocks at Archean-Paleoproterozoic boundary, then two regions stand out: first is the Pechenga - Imandra-Varzuga Greenstone Belt with the Onega Basin of northwestern Russia (Melezhik *et al.*, 2013), and second, the Francevillian Basin of southeastern Gabon (Gauthier-Lafaye and Weber, 1989).

The Francevillian Basin of Gabon contains a volcanic-sedimentary succession of Paleoproterozoic age (Weber, 1968; Gauthier-Lafaye and Weber, 1989). The Francevillian succession is arguably one of the best preserved Paleoproterozoic sedimentary successions that is of late-diagenetic grade (Ossa-Ossa *et al*., 2013) and is only mildly deformed into open folds and cut by high-angle faults (Gauthier-Lafaye and Weber, 1989).

The Francevillian Basin succession records most of the post-GOE events including the LJE but is also known for natural fossil nuclear fission reactors, the earliest putative macrofossils, and also large U and Mn ore resources (El Albani *et al.*, 2010; Weber *et al.*, 2016; Ossa Ossa *et al.*, 2018). However, the age constraints of the succession formation are somewhat poorly

defined. Only ignimbrite tuff beds in the upper part of the stratigraphy have been dated by zircon U-Pb ages (Horie *et al*., 2005) but argued by Weber *et al*. (2016). The depositional age of the lower part of the stratigraphy is roughly delineated by zircon ages of the intruding syenites and granites of the N'goutou Complex (Moussavou and Edou Minko, 2006; Sawaki *et al*., 2017).

The aims of this thesis were, first to learn the zircon U-Pb dating principles and laser-ablation inductively coupled plasma mass-spectroscopy technique (LA-ICP-MS), and secondly to measure the U-Pb and Pb-Pb ages of the zircons separated from putative tuff layers in middle and upper part of the Francevillian stratigraphy by LA-ICP-MS method.

1. Francevillian Basin

1.1. Location and general geology

Francevillian Basin is a geological structure located in the southeast of Gabon on the western margin of Congo Craton. It consists of Archean crystalline basement of granitoid-greenstones and a volcanoclastic-sedimentary Group that lies unconformably on top of that. Eastern part of the series is unmetamorphosed and western part is slightly metamorphosed by tectonic events. Thickness of sediments is about 2 km and the basin covers an area of about 42 000 km^2. The sedimentary succession was formed in the Paleoproterozoic era during the first oxidation of Earth's atmosphere. It is one of the best preserved late-diagenetic successions of its age on Earth. (Gauthier-Lafaye and Weber, 1989)

Francevillian Basin is divided into four sub-basins: Booué, Lastoursville, Okondja and Franceville (Figure 1) (Ossa Ossa *et al.,* 2018). Francevillian Basin is best known because of its mineralized uranium and manganese deposits. These have been of interest for many geological surveys done in the basin. In addition to that, the basin hosts natural nuclear fission reaction zones in the uranium deposits and world's oldest putative macrofossils were found there in 2010. (El Albani *et al.*, 2010; Weber *et al.*, 2016)

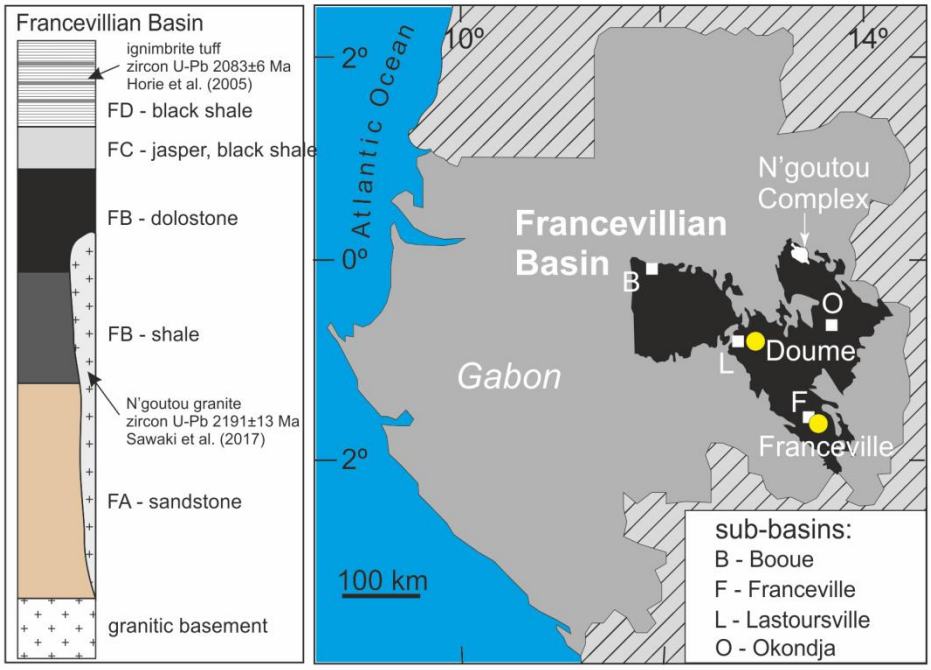

Figure 1. Location of the Francevillian Basin and its sub-basins and general stratigraphy of the succession (modified after Mayika *et al.*, 2021).

The sedimentary succession is divided into five lithological units from FA to FE, FA being stratigraphically the lowest and FE the uppermost unit (Figure 1). The Francevillian A (FA) unit consists of coarse-grained sandstones – detrital deposits of quartz-arenite transported there by flowing water (Weber *et al.*, 2016). Transgressional transition from fluvial to deltaic and beach/shoreline type of sedimentation has taken place during the formation of the FA unit. Mineralized uranium deposits are found in the upper part of this unit in deltaic plane sediments. (Gauthier-Lafaye and Weber, 1989; Bankole *et al*., 2016)

The Francevillian B (FB) formation is divided into two subunits: FB1 and FB2. Lower part of unit FB1 is mainly composed of organic rich black shales and turbiditic sandstones. The upper part of the unit is represented by iron and manganese rich carbonates. The FB2 unit is made of massive sandstones called Poubara sandstones with occasional interlayered black shales. Poubara sandstones are interpreted as turbiditic, deltaic or storm-wave deposits. K-bentonite beds are also found there. The sandstones are capped with organic rich black shales and siltstones. In Booué sub-basin and on the highlands separating Franceville sub-basin from Okondja sub-basin the FB pelitic sandstones and shales are absent. In some areas even FA deposits can be missing, so FC formation lies directly on Archean basement. In the Okondja sub-basin the FA and FB formations are cut by intruding igneous pluton called N'goutou complex. (Weber *et al.,* 2016; Bankole *et al.,* 2018)

The Francevillian C (FC) formation consists of evaporitic dolomites and stromatolitic cherts that are interlayered with black shales. In Franceville and Okondja sub-basins the uppermost layer of the FC unit contains pyroclastic sediments as well. (Weber *et al.,* 2016)

The Francevillian D (FD) unit begins with organic rich black shales interlayered with pyroclastic beds. The tuff beds were produced by explosive volcano eruptions of andesitic to ryolitic magmas. The composition of tuffs are chemically different from magmas that formed N'Goutou intrusions, suggesting that tectonic situation must have changed between formation of FB and FD units. Horie *et al.* (2005) attempted to date the pyroclastic beds by U-Pb dating of zircon grains found from the ignimbrite bed in FD units. The ages spread from 2825 Ma to 2000 Ma, which means at least some of the grains must have been inherited from the Archean basement. On top of the black shales lie sequences of erosional sandstones and pelites. (Weber *et al.,* 2016)

The sedimentary succession of the Francevillian Basin is completed by the Francevillian E (FE) formation that contains two large sequences of sandstones where rare ignimbritic pebbles occur as well. (Weber *et al* 2016)

1.2. Geochronology of the Francevillian Basin

The Archean basement of the Francevillian Basin consists of metamorphosed terrains intruded by plutons that have been dated by U-Pb ages between 2998 ± 25 Ma to 2922 ± 24 Ma (Mouele *et al.,* 2014). N'goutou igneous complex intruding the FA and FB formations in Okondja sub-basin has been dated by Moussavou and Eduo Minko (2006) and Sawaki *et al.* (2017) by zircon grains separated from the granites and syenites yielding U-Pb ages of 2027 ± 55 Ma and 2191 ± 13 Ma, respectively. Therefore, formations FA and FB cannot be any younger because the intrusions intersect with these. (Weber *et al.,* 2016)

Clay fractions of shales intercalating with manganese rich carbonates from FB unit were dated by Bros *et al.* (1992) and Stille *et al.* (1993) using Sm-Nd method yielding ages of 2099 ±115 Ma and 2036 ± 70 Ma. (Weber *et al.,* 2016)

The ignimbrites in FD formation were dated by zircon U-Pb method at 2083 ± 6 Ma by Horie *et al*. (2005). However, Weber *et al.* (2016) expressed doubts on these ages because the age was received from a mix of two populations of zircons with different ages. One population yielded ages from 2136 to 2068 Ma and the second one from 2042 to 2003 Ma. Weber *et al.* (2016) suggested that the older set was most possibly obtained from the basement whereas younger ages may reflect the true sedimentation age of tuff beds. (Weber *et al.,* 2016)

In addition to the radioactive decay methods the Francevillian succession has been correlated to the Paleoproterozoic sedimentary basins worldwide using carbon isotope excursions that have often been used to correlate different sedimentary strata of same age from all over the world. The Paleoproterozoic after the Great Oxidation Event is marked by the longest-lived and highest amplitude carbon isotopic excursion – the Lomagundi-Jaguli Event (LJE) that is also recorded in carbonates of the Francevillian Basin linking the sediments to the LJE (Weber and Gauthier-Lafaye, 2013; Preat *et al.,* 2011). However, Bakakas-Mayika *et al.* (2021) have recently shown that carbon isotope excursion in Lastrousville sub-basin is facies related and the use of this event as a global stratigraphic correlation tool calls for caution.

2. Zircon dating

2.1. Radioactive decay and dating techniques

Radioactive dating is based on disintegration of unstable atoms. This means that an unstable isotope of an element loses particles during a decay event and eventually takes a stable form. (Vermeesch, 2017)

Atoms consist of nucleus and electrons orbiting around nucleus in a diffuse cloud. Nucleus is made of protons and neutrons that together define the mass number of an element. The number of protons in an element is fixed but the number of electrons and neutrons may vary. The variation in the number of electrons is what produces ions with different electrical charge and the variation in the number of neutrons is what produces isotopes with different mass. One proton can stabilize a certain number of neutrons so that any number lower or higher than the given limit results in the element being unstable and thus becoming radioactive. The number of neutrons stabilized by one proton varies in different elements, being close to 1 in elements with lower mass number and higher in heavier elements. (Vermeesch, 2017)

Unstable forms of elements go through radioactive decay to become stable. There are different disintegration mechanisms. First is the α-decay, where the nucleus of an element loses an α-particle. When the α-particle acquires electrons, they turn into He-atoms. The U-Th-He chronothermometer is based on that decay principle. The recoil energy from the loss of α-particle is partly acquired by the parent nucleus, which then emits γ-radiation to relax back into its ground state. Energy levels of α-particles are discrete. α-decay is the main form of disintegration in ^{147}Sm-^{143}Nd, ^{235}U-^{207}Pb, ^{238}U-^{206}Pb and ^{232}Th-^{208}Pb decay series. (Vermeesch, 2017)

If the element goes through β-decay, negatron (β^-) or positron (β^+) is emitted from nucleus. The energy carried by β-particles can be described with continuous energy spectrum. Negatron decay is important for the ^{40}K-^{40}Ca, ^{87}Rb-^{87}Sr and ^{14}C-^{14}N systems and occurs in ^{235}U-^{207}Pb, ^{238}U-^{206}Pb and ^{232}Th-^{208}Pb decay series as well. In negatron decay the element loses a neutron and gains a proton. Positron decay is central in ^{40}K-^{40}Ar system, where the element loses a proton and gains a neutron. β-decay is also accompanied with γ-radiation to relax the parent nucleus and to annihilate the unstable positron in positron decay. (Vermeesch, 2017)

Electron capture and nuclear fission mechanisms can also be used for geochronological analysis. Electron capture is similar to positron emission and they often occur together. Nuclear fission occurs in disintegration of large nucleus when two unequally sized daughter nuclei start moving in different directions and damage the structure of the host mineral in process. Daughter isotopes are radioactive as well and go through β-decay later to become stable. For dating the sample, frequency of fission tracks in host mineral is measured. Nuclear fission is not very common decay mechanism, occurring naturally in larger quantities only in ${}_{92}{}^{238}\mathrm{U}$ and even there α-decay events are far more common. (Vermeesch, 2017)

Radioactive decay is not related to changes in external environments, thus it can be used as a reliable age detection method. The rate of radioactive decay is dependent only on the number of parent atoms present in the beginning of the disintegration. If the number of parent atoms in the sample at present and time 0 (in the beginning of the decay) is known, the time from the beginning of the radioactive decay until the present can be found from the following equation:

$$P = P_0 e^{-\lambda t},$$

where P is the number of parent atoms present in the sample, P_0 is the number of parent atoms at time 0 and λ is decay constant for the given series. (Vermeesch, 2017)

Usually, the number of parent atoms at time 0 is not known. If D is the number of daughter nuclei present in the sample, then $P_0 = P + D$. Therefore, the equation

$$t = \frac{1}{\lambda} \ln\left(\frac{D}{P} + 1\right)$$

can be used to calculate the time of radioactive disintegration. The more daughter element in the sample, the older the sample is. To receive reliable age data, it must be taken into consideration if there was any number of daughter nuclei in the sample before the radioactive disintegration began. In addition to that, it is important that the system has been closed, so no daughter or parent nuclei have been lost or added. (Vermeesch, 2017)

2.2. Radioactive dating of zircon

Zircon grains are often used for radioactive dating because they are quite durable to any alteration from outer sources. They are common accessory minerals in felsic igneous rocks, so they can be used to date the age of an igneous or metamorphic complex or to define the source of sediment carried into basin. (Vermeesch, 2017) Zircon has high U and Th concentrations making it suitable for geological dating. This is because crystallization of zircon starts in high temperature magma and lasts until the end phases of cooling. In the end, magma is enriched with incompatible elements including U^{4+} and Th^{4+} which are then incorporated into minerals such as zircon, substituting Zr^{4+} in the zircon crystal structure. At the same time Pb isotopes that are the stable end-members of the U and Th decay but have 2+ valence are not incorporated into zircon structure because of the crystallochemical restrictions. (Villa *et al.*, 2017)

There are several techniques to measure the isotopic composition of the sample. For liquid or dissolved samples thermal ionization mass spectrometry (TIMS) is used. The solution is heated to the point of vaporization and ionization. Formed ions are separated based on their mass-charge ratio and measured with a mass-spectrometer. This technique provides the most accurate chemical composition of the sample but does not have spatial resolution so it cannot be used for heterogenous samples. (White, 2015)

Most of the geological samples are homogenous only on a very small scale. For heterogenous samples, different microbeam dating techniques are used. One of them is secondary ionization mass spectrometry (SIMS) which uses ion beam to evaporate material from the surface of the sample. The vapor is ionized and ion concentrations measured with mass-spectrometer. Isotope ratios provided by SIMS are less precise than with TIMS but because of the possibility to analyse a small homogenous part of the sample, the yielded age may be more accurate. SIMS is not used very widely due to the cost of machinery and operators. (White, 2015)

Laser-ablation inductively coupled plasma mass-spectrometry (LA-ICP-MS) is another common microbeam dating technique. It allows analysis of discrete parts of the sample just as SIMS. The cost of an analysis is lower than for TIMS and SIMS but the resolution of this technique is not as good. (Košler, 2007)

2.3. U-Pb dating

Several U and Th decay series are used in geochronology. These are long series where the first parent nuclide is ^{235}U, ^{238}U or ^{232}Th. The series consist of many α and β^- disintegrations because daughter atoms of first decays are unstable. The final isotope for ^{235}U series is ^{207}Pb, for ^{238}U series it is ^{206}Pb and ^{208}Pb for ^{232}Th series. (Vermeesch, 2017)

Four Pb isotopes occur in nature: ^{204}Pb, ^{206}Pb, ^{207}Pb and ^{208}Pb. Of those, three last ones are radiogenic meaning they cannot originate from any other source than radioactive decay. If there is no ^{204}Pb in the sample, the suitable decay series can be used to calculate the age of the sample. If ^{204}Pb has been inherited from the environment during mineral formation or later, calculations must be normalized to it, otherwise the Pb/U ratio provided by analysis would be higher than it really is. (Vermeesch, 2017)

The $^{207}Pb/^{206}Pb$ ratio can also be used for dating. It is based on the isotopic concentrations of lead in the sample and average natural $^{238}U/^{235}U$-ratio, which equals 137.818. Choice of method depends on predicted age of the samples. For older samples, it is advised to use $^{207}Pb/^{206}Pb$ method, for younger samples $^{238}U/^{206}Pb$ system is more reliable. This is because $^{207}Pb/^{206}Pb$ ratio is the least sensitive to any kind of changes in chemical composition of the sample. While U and Pb concentrations can change differently due to U being mobile in some chemical situations, there is not much fractionation between different Pb isotopes during influx or efflux of lead. Based on empirical analyses, it is advised to use $^{207}Pb/^{206}Pb$ method for samples older than 1.5 Ga and $^{206}Pb/^{238}U$ method for younger samples (Figure 2). (Vermeesch, 2017; Spencer *et al.,* 2016)

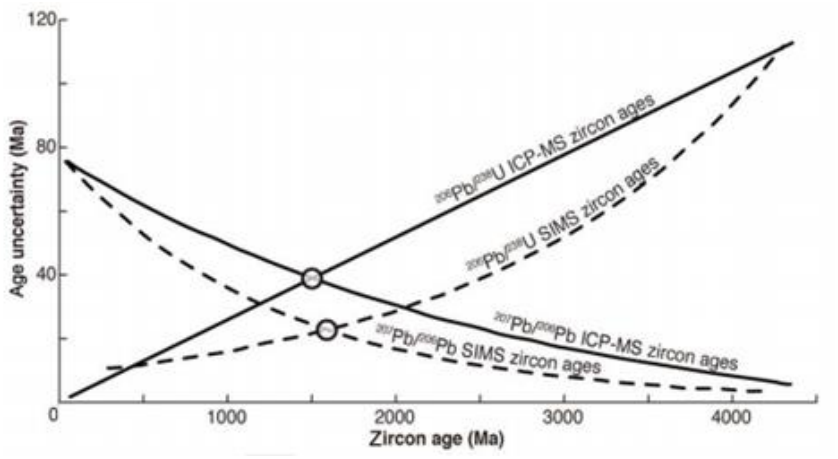

Figure 2. The age uncertainty relative to the age of the sample in $^{206}Pb/^{238}U$ and $^{207}Pb/^{206}Pb$ methods (from Spencer *et al.*, 2015).

The results of different U-Th-Pb series can provide different results in one sample. When ratios of $^{206}Pb/^{238}U$ and $^{207}Pb/^{235}U$ that yield the same age are plotted on a diagram, they form the so-called Wetherhill concordia curve (Figure 3a). If the system has been open and a change in the isotopic composition of the sample has occurred, the data does not plot on the concordia curve. The most common change is loss of radiogenic Pb, which results in the dataset being plotted below concordia curve on a discordia line (Figure 3a, yellow data points). This is a line that intersects with the curve in points of expected crystallization age of the mineral (upper intersection) and the expected time of Pb loss (lower intersection). If the loss of radiogenic Pb has been recent in geological timescale, the lower intersection point is approximately at time 0 (i.e., present day) (Figure 3a, blue data points). If radiogenic Pb is gained from the environment or U escaped, the data plots on discordia line but higher than the upper intersection. Non-radiogenic Pb (i.e., common lead) gain results in the data being plotted to the right from discordia line. (Villa *et al.*, 2017)

Figure 3b shows Tera-Wasserburg concordia diagram, which is generated by plotting the ratios of $^{206}Pb/^{207}Pb$ and $^{206}Pb/^{238}U$ on a diagram. Similarly to the first the open system processes result in deviation of the data from the concordia. (Villa *et al.*, 2017)

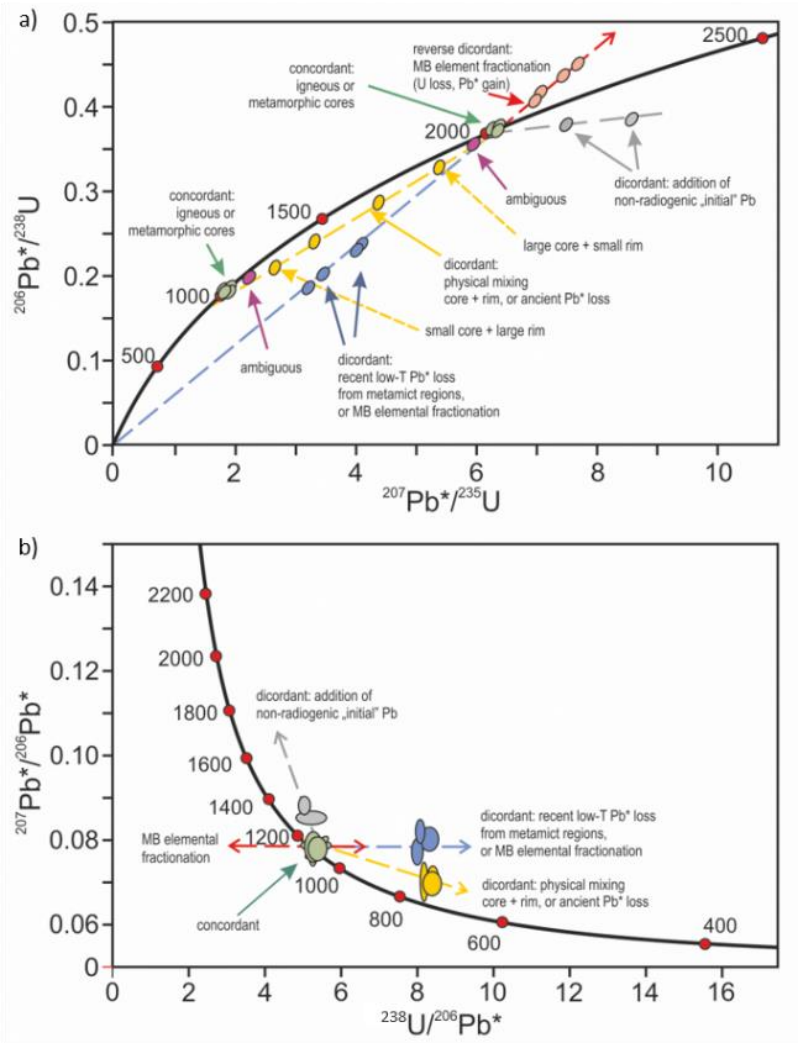

Figure 3. (a) Example of the Wetherhill concordia curve with possible causes of discordia augmented. (b) Example of the Tera-Wasserburg concordia curve with possible causes of discordia augmented. (after Villa *et al.*, 2017)

2.4. Laser-ablation method in dating

Inductively coupled plasma mass-spectrometry (ICP-MS) is a method used to measure concentration of elements on the level of trace elements (depending on the element 0.01…0.001 µmol/L). ICP-MS is originally designed for measuring liquid samples. Solid samples can be measured using electrochemical vaporization or laser-ablation. (Wilschefski and Baxter, 2019)

Laser-ablation part of the laser-ablation inductively coupled plasma mass-spectrometry (LA-ICP-MS) system consists of four parts: a laser, that generates frequent pulses of high-energy photons; delivery system to modify the laser beam parameters and guide it to the surface of the

sample; ablation cell where the beam interacts with the sample surface and a transportation system to take the aerosol from ablation cell to the ICP part of the system. (Košler, 2007)

ICP itself is the ion source of the system. Plasma is formed by heating a noble gas (usually Ar, combined with He) to temperatures so high that ionization process begins. The aerosol formed in ablation is transported into plasma, and this is where the sample gets ionized. (Wilschefski and Baxter, 2019)

Ion beam is sent through nickel or platinum cones to a high vacuum chamber and guided forward to ion optics system. The system consists of charged surfaces and guides the ion beam to mass-spectrometry system. The ions in the beam are divided by their mass-charge ratio in a mass-filter. The filtered beam is then guided to mass-spectrometer where the intensity of the beam is converted into an electrical signal to be measured. (Longerich, 2008; Wilschefski and Baxter, 2019)

LA-ICP-MS technology has several advantages compared to other techniques used for measuring the concentration of elements in the sample. First, different elements in the sample can be measured during one analysis. In addition to that, the amount of sample necessary for analysis is relatively small and the process of preparation is simple. LA-ICP-MS allows the mineral grains to be measured *in situ*, so the grains do not necessarily need to be extracted from the surrounding rock. The cost of one analysis is lower than that for SIMS or TIMS, and less time-consuming. For this reason, LA-ICP-MS is often used in studies with large number of samples. (Košler, 2007)

3. Material and methods

Material for this study was obtained from Francevillian Basin, Gabon. Three samples FRA-Zr-01, FRA-Zr-02 and FRA-Zr-03 are from presumed tuff layers in FB1 black shales outcropping at the side of the Independence Square, Franceville town (Figure 4).

Samples were collected and screened after heavy mineral fraction separation for zircons at Masuku University, Franceville.

Figure 4. Outcrop of the FB2 formation shales at the side of the Independence Square, Franceville in 2017. (A) General overview of the outcrop. (B) tuff-like layer in the black shale. Photo by K. Kirsimäe.

Fourth and fifth samples (DM57 and DM136) were derived from a K-bentonite bed in FD Formation intersected in Doume drillcore in Lastrousville sub-basin (Figure 1). Sample DM57

is from 29.0 m and sample DM136 from 55.7 m depth in Doume drillcore (Figure 5) where series of greenish beige K-bentonite beds occur. A few cm-thick bentonite beds are composed of illitic K-mica and mixed layer illite-smekctite mineral with traces of quartz and feldspar (Peeter Somelar, personal communication, 2021).

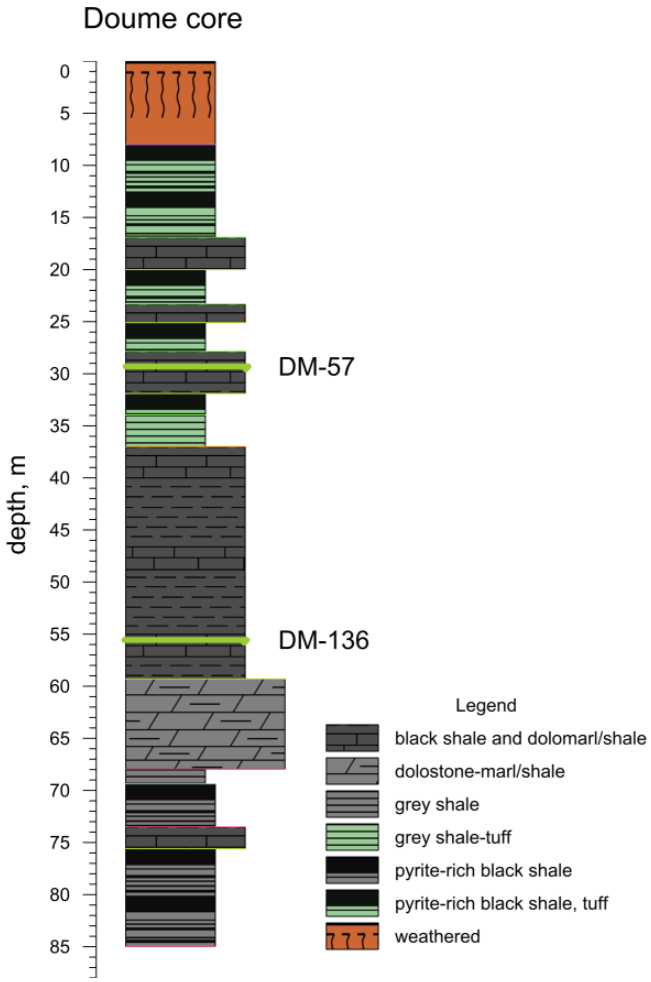

Figure 5. General lithology of the Doume drillcore and location of the studied samples. Lithology description by K. Paiste.

The Doume samples were dispersed in distilled water using ultrasonic bath and the clay fraction was removed by repeated washing. The collected grains were fractionated in heavy liquid (density 2.89 g/cm^3) and zircon grains were picked under binocular. In DM57 sample no measurable zircon grains were found. The grains were placed on double-sided tape and embedded in epoxy resin. The sample was polished using sandpaper (grit size 2500) and diamond suspensions (sizes 6 µm, 3 µm and 1 µm). The samples were photographed using Leica DM 2500P optical microscope (Figure 6).

Scanning electron microscopy (SEM) imaging of mounted grains was done using a ZEISS EVO MA15 SEM. The images were captured by backscattered electron (BSE) and in variable pressure (VP) mode and chemical characterization by elemental mapping of the samples was carried out with Oxford AZTEC-MAX energy-dispersive spectroscopy (EDS) attached to SEM. The VP mode enables charge contrast imaging of uncoated samples where SEM images are collected from signals arising from bombardment of a sample with an electron beam where non-conductive samples begin to charge (Üpraus, 2014). In non-conductive samples the differences in material dielectric properties and structural defects and/or impurities and vacancies can act as electron traps creating an image where brighter areas correspond to high electron trap densities. Charge contrast imaging is similar to cathodoluminescence (CL) imaging (Griffin, 2000; Watt *et al*., 2000). Charge contrast imaging was done to reveal the growth zones and dislocations in zircon crystals.

The U and Pb isotopic composition of the samples was measured in four sessions using Agilent 8800 inductively coupled plasma mass-spectrometer coupled to a Cetac LSX213 G2+ laser and HelExII ablation cell. Measurements were carried out using 40 µm spot size, 5 Hz repetition rate and fluence of 1.5 J/cm^2 for larger grains in samples FRA-Zr-01, FRA-Zr-02 and FRA-Zr-03. Laser spot size 20 µm, 5 Hz repetition rate and fluence of 1.9 J/cm^2 was used for smaller grains in Doume sample. Ablations lasted for 50s and were preceded by 20s of background measurements. Masses ^{178}Hf, ^{202}Hg, ^{204}Pb, ^{206}Pb, ^{207}Pb, ^{208}Pb, ^{232}Th and ^{238}U were measured using dwell times of 5.5, 5.1, 10, 9.5, 200, 10, 10 and 40 ms respectively, corresponding to a total duty cycle of 400 ms. International zircon standard 91500 was used for calibration and *in-house* standard Scottish Small described in Ausmeel (2020) were used for quality control. Data reduction was done in program Iolite 3.36 and MS Excel Isoplot 4.15 was used to analyse concordance of the results.

4. Results

Optical and SEM imaging

Morphology of zircon grains was analysed using optical and SEM imaging (Figures 6, 7, 8, 9, 10). Most of the grains were fractured and some had growth zones recognisable in SEM images. Grains that had distinguishable core and rim usually provided different age data from the core and the rim, the core being older. There were grains that had inclusions of other minerals (e.g., apatite) in them (Figure 10). Zircons in sample DM136 were roughly two times smaller than grains in other samples.

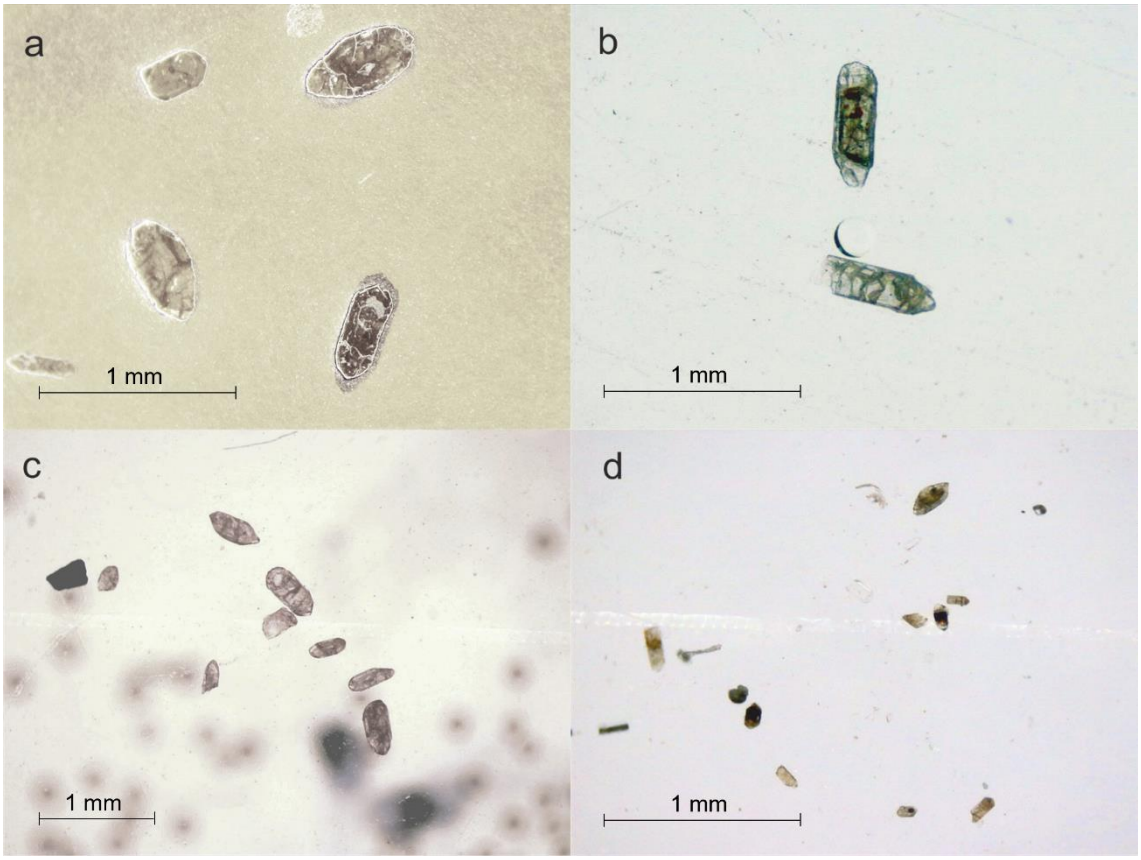

Figure 6. Selection of optical images of all samples. (a) sample FRA-Zr-01; (b) sample FRA-Zr-02; (c) sample FRA-Zr-03 and (d) sample DM136.

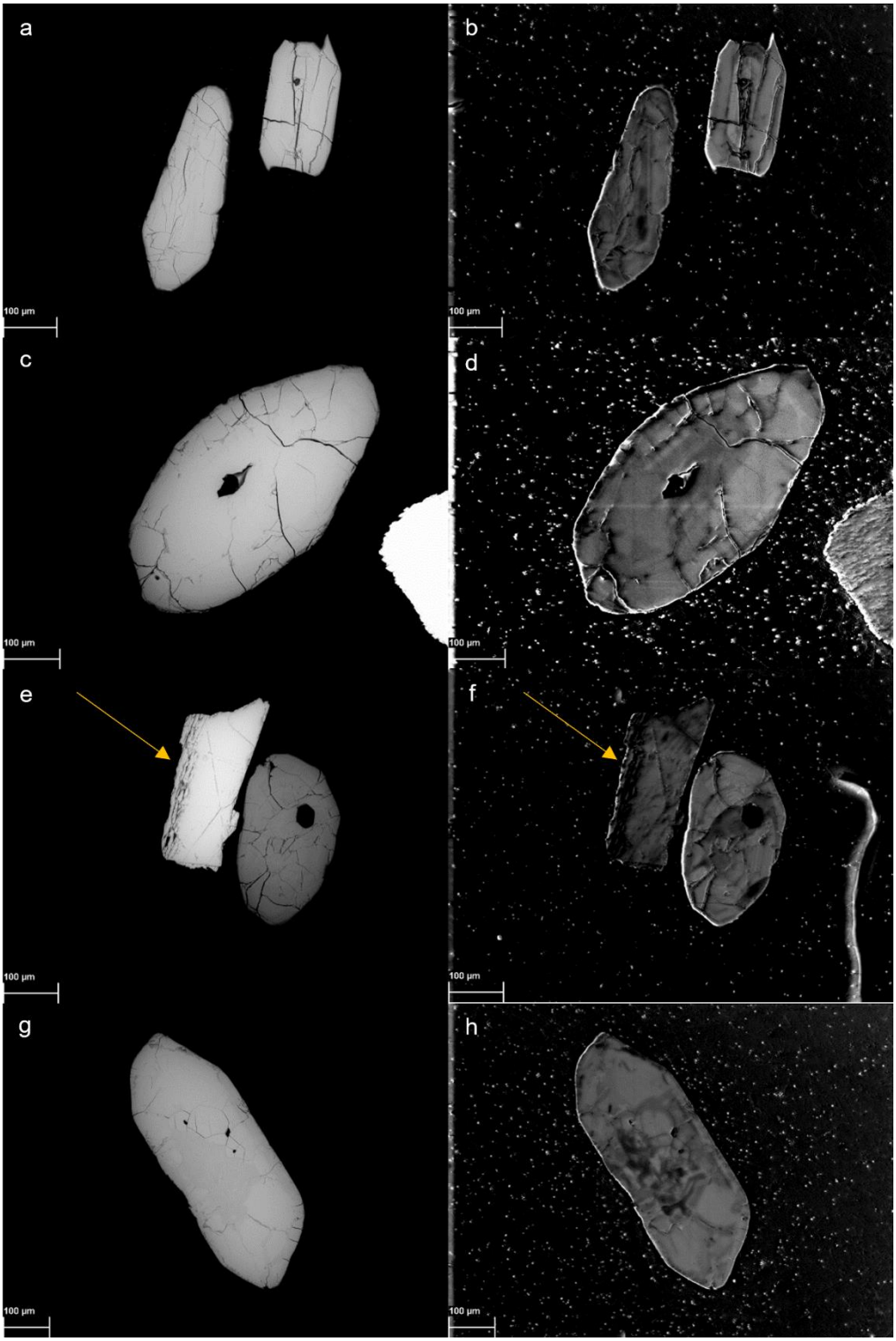

Figure 7. SEM images of zircons in FRA-Zr-01 sample. Images (a), (c), (e) and (g) are taken in BSE mode; figures (b), (d), (f) and (h) are taken in VP mode. Yellow arrows on images (e) and (f) point to a monazite grain.

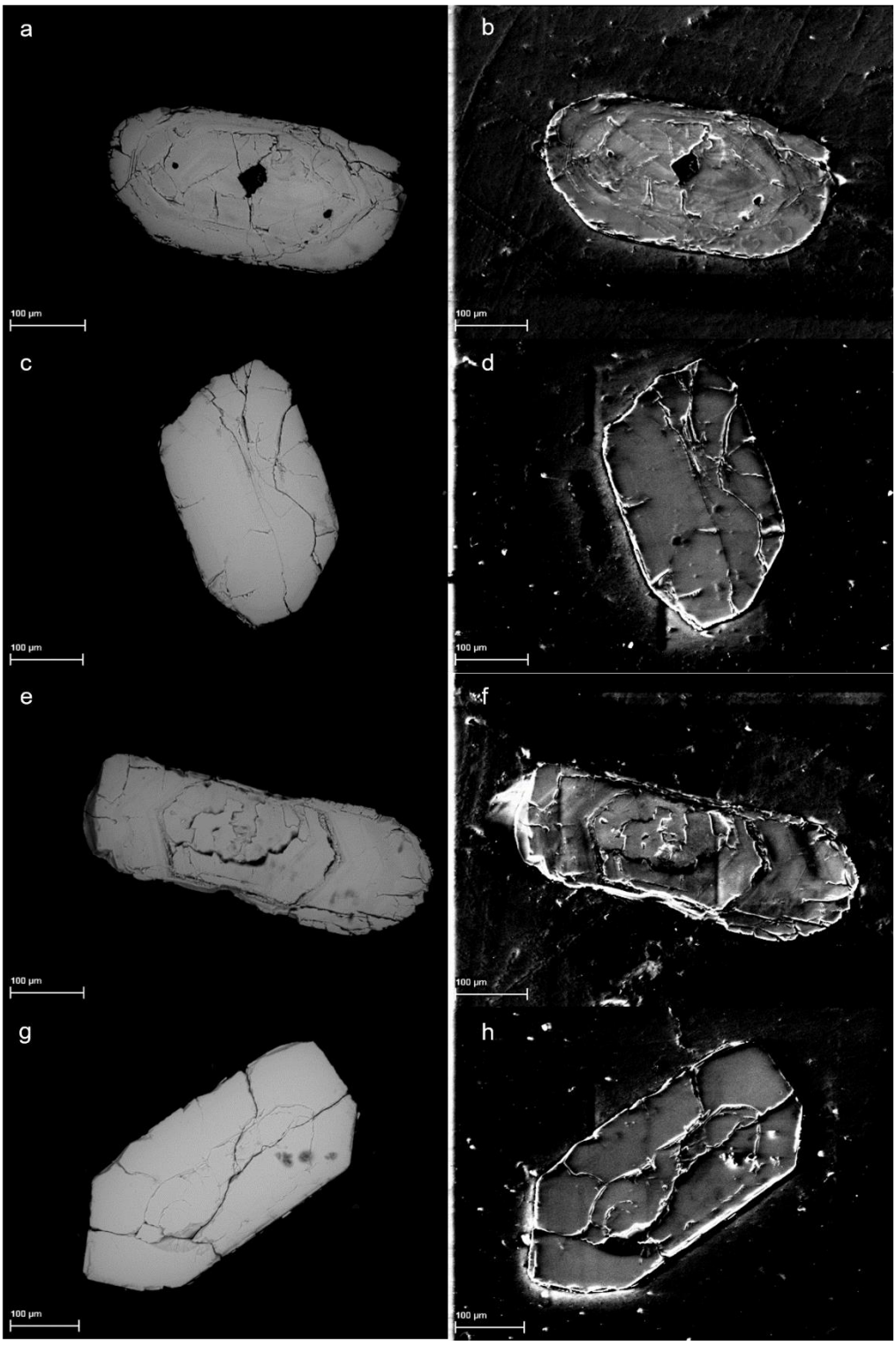

Figure 8. SEM images of zircons in FRA-Zr-02 sample. Images (a), (c), (e) and (g) are taken in BSE mode; figures (b), (d), (f) and (h) are taken in VP mode.

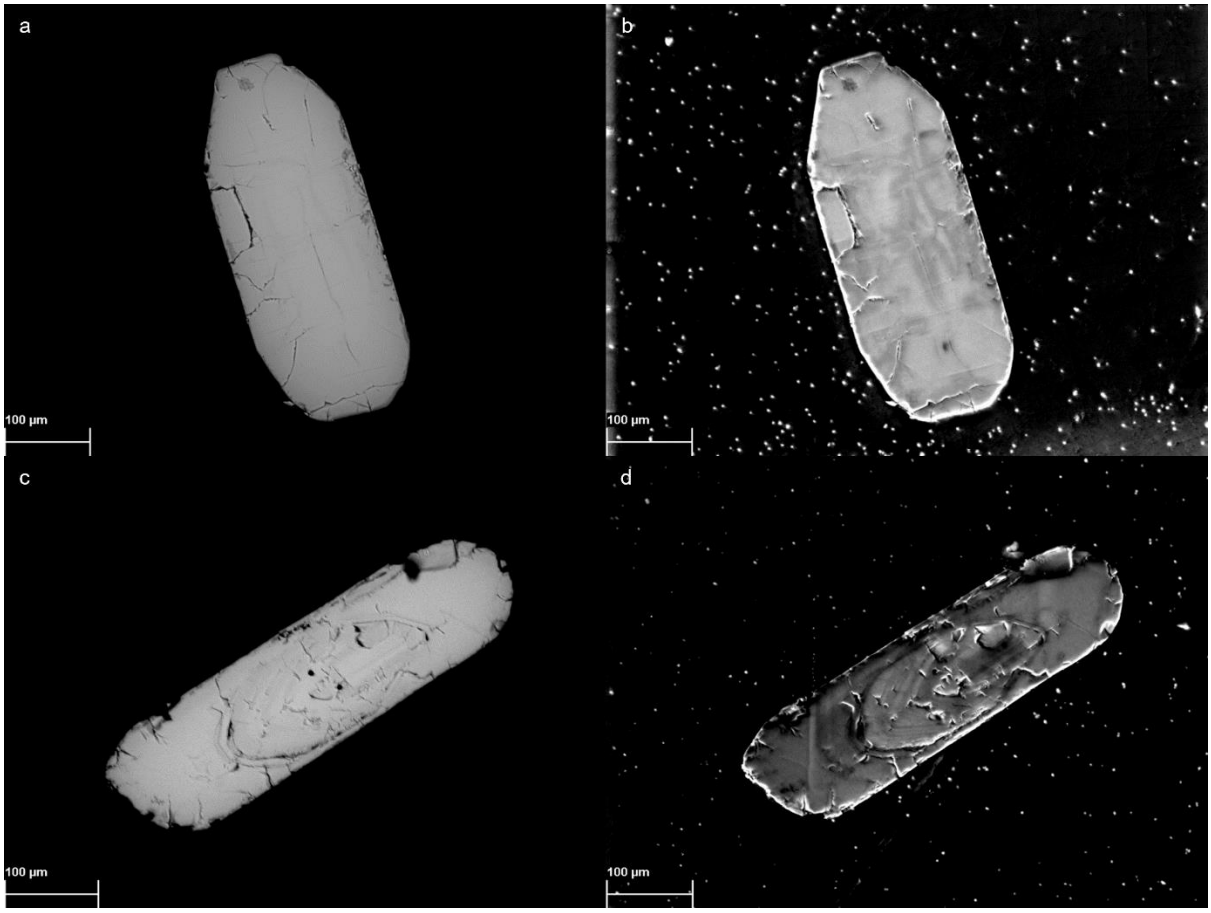

Figure 9. SEM images of zircons in FRA-Zr-03 sample. Images (a) and (c) are taken in BSE mode; images (b) and (d) are taken in VP mode.

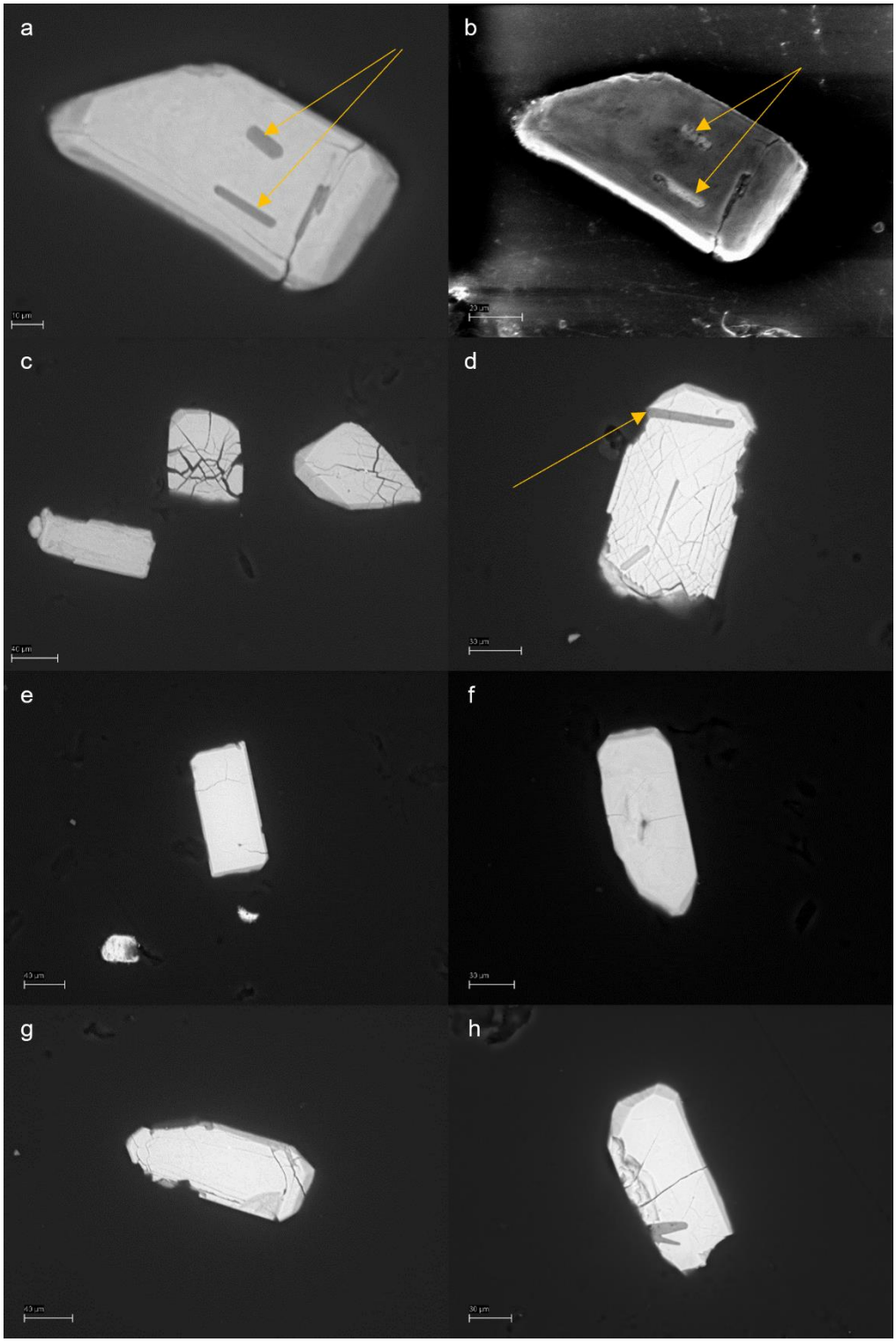

Figure 10. SEM images of zircons in DM136 sample (a-h). Image (b) is taken in VP mode, others are taken in BSE mode. Yellow arrows on images (a), (b) and (c) point to apatite inclusions in zircon grains.

LA-ICP-MS dating

Concentrations of U and Pb isotopes were measured in each zircon grain. Data reduction was done using Iolite 3.36. Both Wetherhill and Tera-Wasserburg concordia diagrams were plotted in MS Excel Isoplot 4.15.

The reliability of the results was evaluated based on three criteria: intensity of common lead (^{204}Pb) signal; visual interpretation of signal spectrums for ^{207}Pb/^{235}U, ^{206}Pb/^{238}U and ^{207}Pb/^{206}Pb final age data and concordance filtering based on the ratio of ^{206}Pb/^{238}U and ^{207}Pb/^{206}Pb. If the difference of final age by ^{206}Pb/^{238}U and final age by ^{207}Pb/^{206}Pb method was more than 10%, it was decided that the data point is an outlier. Data was colour-coded on concordia diagrams. Black ellipses indicate reliable age data. Blue data points display grains that had high intensity of common lead signal. Red data points display outliers based on concordance filtering and purple ellipses represent data with unstable signal spectrums. The choice of criteria followed the line (in decreasing order of importance): common lead > concordance filter > unstable spectrum. If concordance filtering result exceeded the threshold and signal spectrum was unstable, concordance filter was considered more reliable method for outlying data; if the intensity of ^{204}Pb signal was high as well, common lead method was considered the most reliable. For DM136 sample threshold of concordance filtering was 20% because there were no grains in the sample for which the filtering result was under 10%.

Sample FRA-Zr-01

In total 18 zircon grains were measured for their U-Pb age in sample FRA-Zr-01 (Appendix 1). Two measurements were done in one grain with distinguishable core and rim. Based on the three criteria for discarding outliers, nine measurements in the sample were reliable (Figure 11, Appendix 1). Six were outliers due to high signal intensity of common lead, three due to unstable signal spectrums and two because the difference in ^{206}Pb/^{238}U and ^{207}Pb/^{206}Pb final ages was more than 10% (Figure 11a,b). For reliable data discordia line on Wetherhill concordia diagram (Figure 11c) has upper intersection with concordia curve at 2766 ± 65 Ma and lower intersection at 1036 ± 860 Ma. For Tera-Wasserburg diagram based on reliable data (Figure 11d) the upper intersection plots at 2749 ± 82 Ma and lower intersection at 1269 ± 870 Ma.

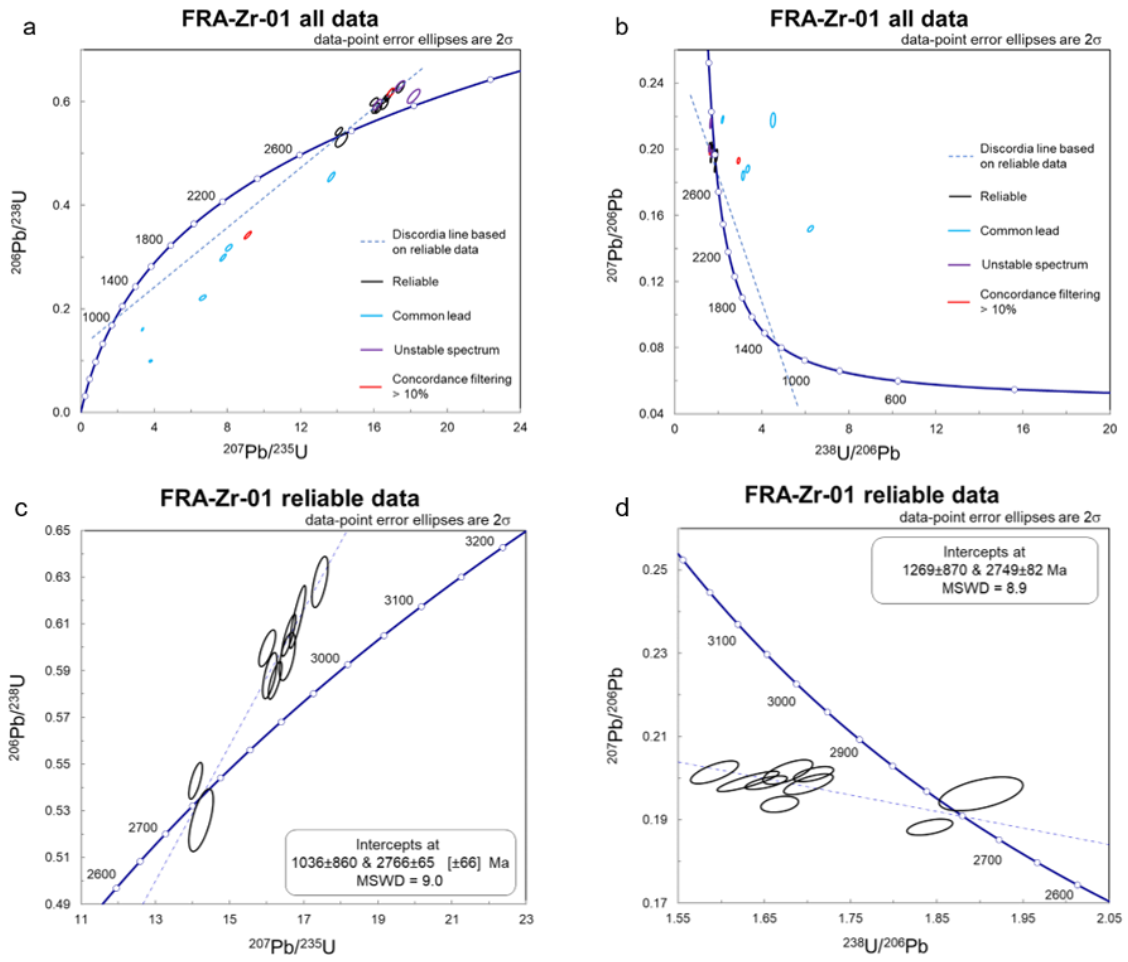

Figure 11. Concordia diagrams for sample FRA-Zr-01. In figures (a) and (b) all acquired data are shown, unreliable datasets are colour-coded (see explanation in the text). In figures (b) and (d) show data points only for reliable analyses.

Relative probability density plot of zircons classified as reliable (Figure 12) shows ages varying between 2780 Ma and 2860 Ma with maximum approximately between 2810 to 2830 Ma.

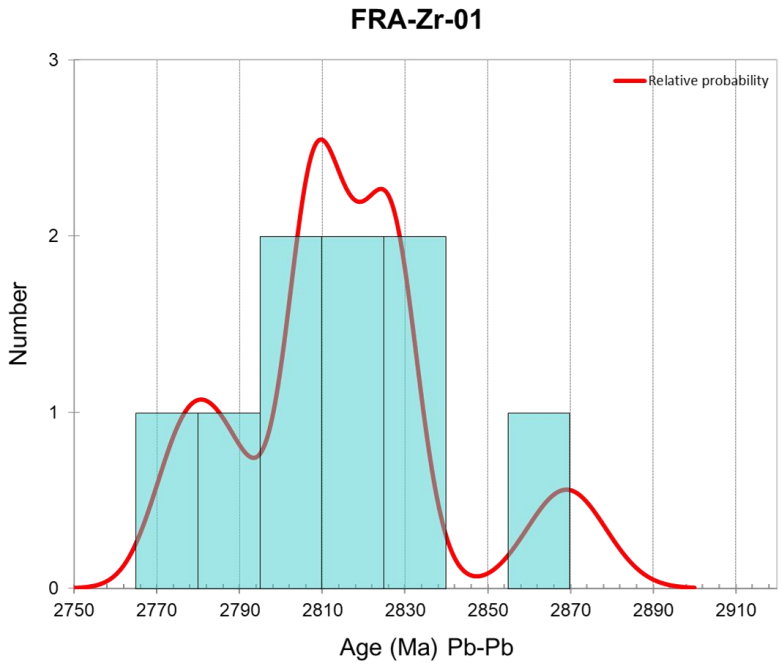

Figure 12. Relative probability of $^{207}Pb/^{206}Pb$ ages in sample FRA-Zr-01 based on analyses classified as reliable data.

Sample FRA-Zr-02

In total 30 grains were analysed in sample FRA-Zr-02 (Appendix 2). There were four grains for which two measurements were done because they had distinguishable core and rim. Based on the three criteria for discarding outliers, 16 measurements were found reliable (Figure 13). Two were outliers due to high signal intensity of common lead, two due to deviations in signal spectrums and 14 because the difference in $^{206}Pb/^{238}U$ and $^{207}Pb/^{206}Pb$ final ages was more than 10%. Using reliable data, discordia line on Wetherhill concordia diagram (Figure 13c) has upper intersection with concordia curve at 2884 ± 59 Ma and lower intersection at 573 ± 3000 Ma. For Tera-Wasserburg diagram (Figure 13d) the upper intersection plots at 2902 ± 22 Ma.

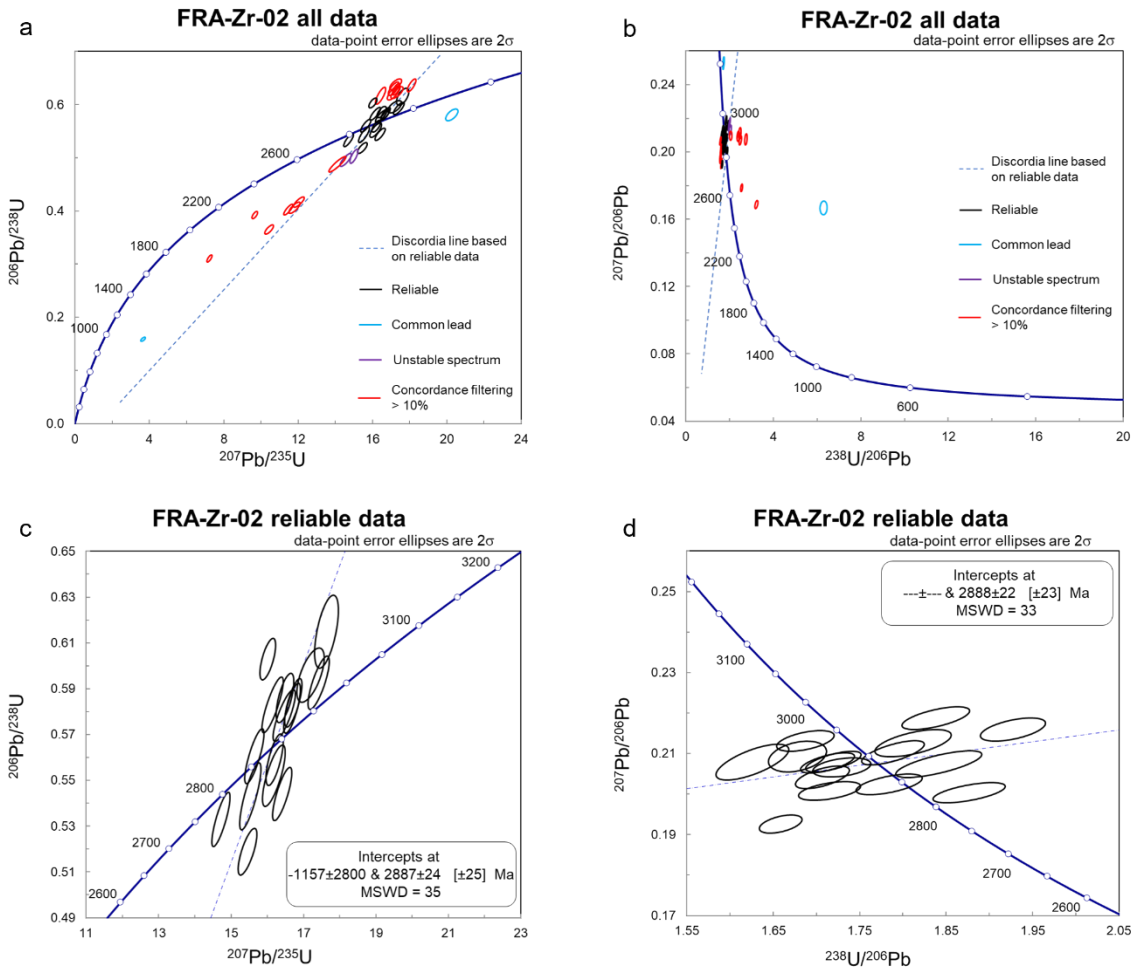

Figure 13. Concordia diagrams for zircons in sample FRA-Zr-02. In figures (a) and (b) all acquired data are shown, unreliable datasets are colour-coded (see explanation in the text). In figures (b) and (d) only reliable data are shown.

Relative probability density plot of reliable data (Figure 14) sets the most probable age of the sample approximately from 2800 to 2840 Ma but a sub-population at 2900 Ma is also apparent.

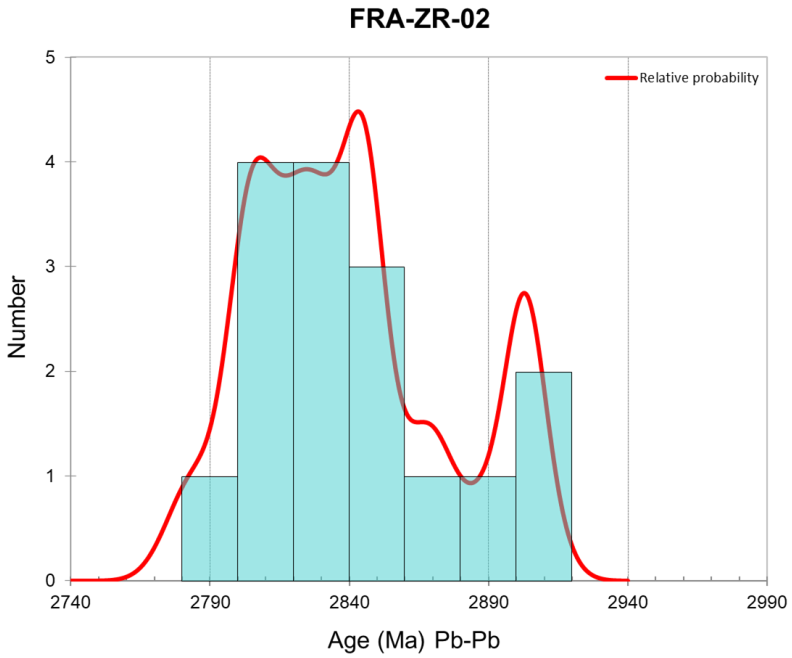

Figure 14. Relative probability of $^{207}Pb/^{206}Pb$ ages in sample FRA-Zr-02 based on analyses classified as reliable.

Sample FRA-Zr-03

In total 18 grains were analysed in this sample (Appendix 3). Two measurements were done in two grains with distinguishable core and rim. Based on the three criteria for discarding outliers, six measurements were found reliable. Seven were outliers due to high signal intensity of common lead, four due to unstable signal spectrums and five because the difference in $^{206}Pb/^{238}U$ and $^{207}Pb/^{206}Pb$ final ages was more than 10%. Using reliable data, discordia line on Wetherhill concordia diagram (Figure 15c) has upper intersection with concordia curve at 2875 ± 26 Ma and lower intersection at -1242 ± 4800 Ma. For Tera-Wasserburg diagram (Figure 15d) the upper intersection plots at 2881 ± 25 Ma.

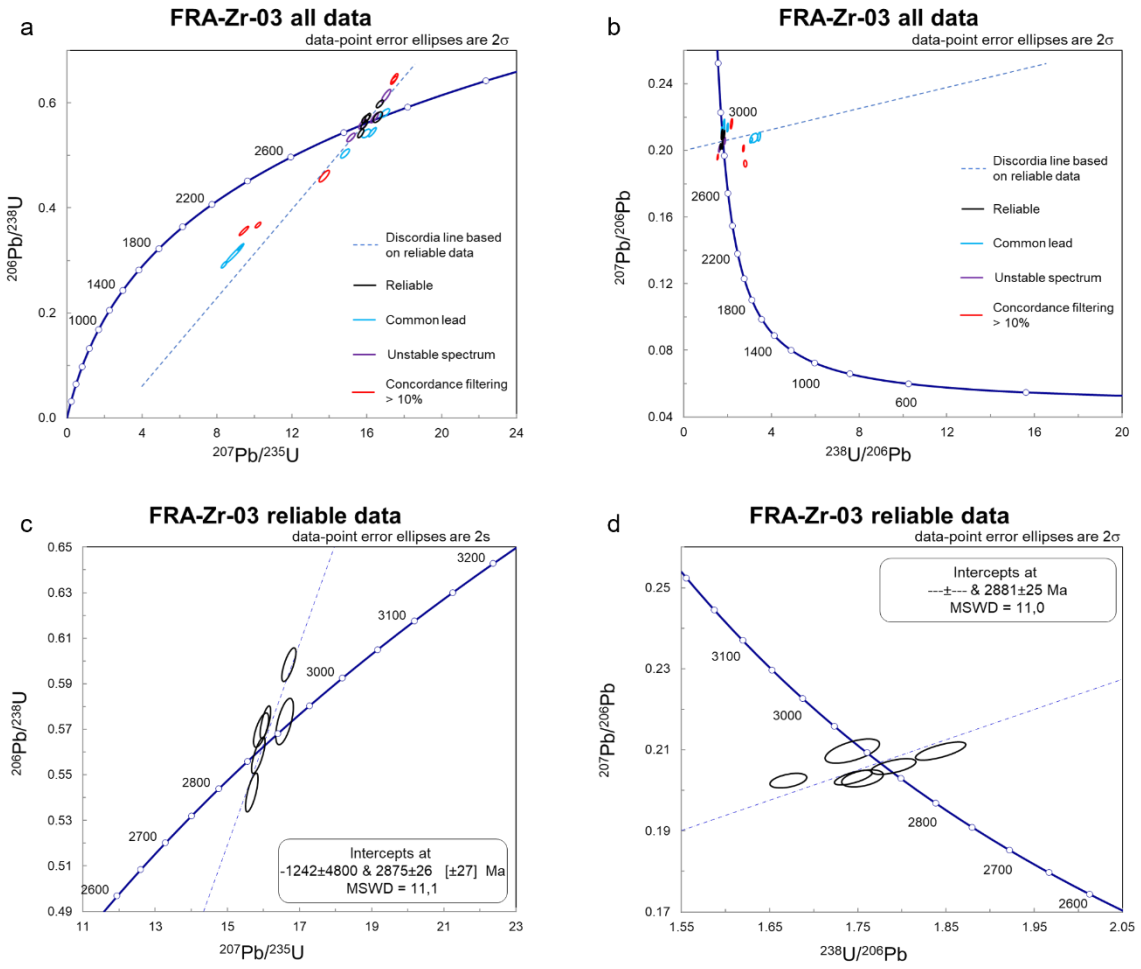

Figure 15. Concordia diagrams for sample FRA-Zr-03. In figures (a) and (b) all acquired data are shown, unreliable datasets are colour-coded (see explanation in the text). In figures (b) and (d) show data points only for reliable analyses.

Relative probability density plot of reliable data (Figure 16) shows the age of the zircons at approximately 2870 Ma and few grains have age between 2910 – 2930 Ma.

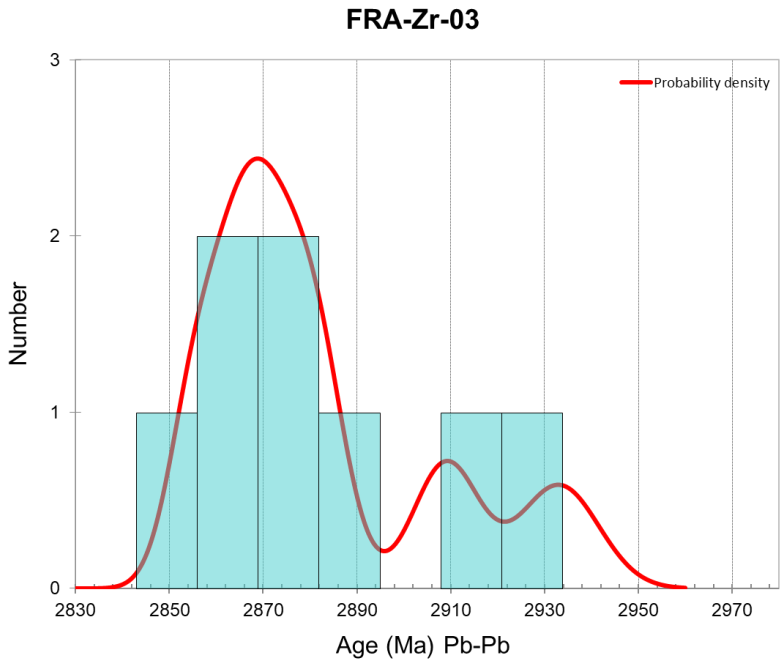

Figure 16. Relative probability of $^{207}Pb/^{206}Pb$ ages in sample FRA-Zr-03 based on reliable analyses.

Sample DM136

In DM136 sample in total 23 zircon grains were analysed (Appendix 4). In some grains, where possible, several measurements were done. Based on the three criteria for discarding outliers, six measurements were reliable. Four were outliers due to high concentrations of common lead, two due to unstable signal spectrums and 28 because the difference in $^{206}Pb/^{238}U$ and $^{207}Pb/^{206}Pb$ final ages was more than 20%. There were no grains for which concordance filter would have been less than 10%. Using the most reliable data, discordia line on Wetherhill concordia diagram (Figure 17c) has upper intersection with concordia curve at 3076 ± 140 Ma and lower intersection at 1553 ± 55 Ma. For Tera-Wasserburg diagram (Figure 17d) the upper intersection plots at 3074 ± 140 Ma and lower intersection at 1553 ± 56 Ma.

Two laser sessions were done for this sample. On first session, laser beam with spot size 20 µm was used because most of the grains in the sample were too small for bigger spot size. On second session only two grains - DM136-20 and DM136-21, that provided most reliable data on first session, were analysed. This time 40 µm spot size was used.

Data from second session revealed that both grains had regions with high concentration of ^{204}Pb. This resulted in only one signal spectrum being stable. This stable signal from zircon grain DM136-20 yields final Pb-Pb age at 2082 ± 19 Ma.

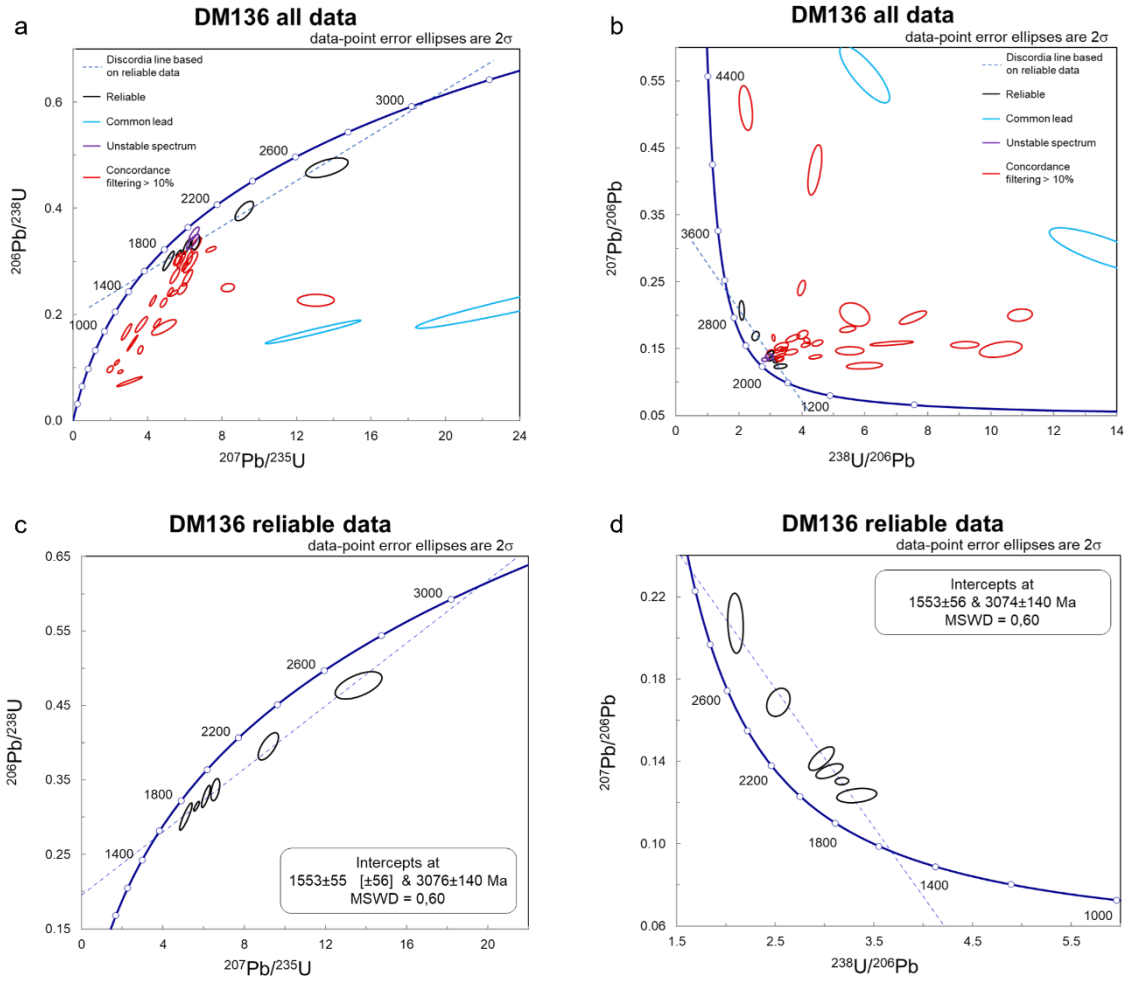

Figure 17. Concordia diagrams for sample DM136. In figures (a) and (b) all acquired data were used, unreliable datasets are colour-coded (see explanation in the text). In figures (b) and (d) only the most reliable data are shown.

5. Discussion

In all samples were numerous zircon grains that did not plot on concordia curve nor on reliable discordia line (Figure 18). This could be interpreted as a change in isotopic composition of the grains. Also, in all FB2 formation samples there were indications of Pb* (i.e., radiogenic Pb) gain (see yellow arrows in Figure 18). However, this type of discordance is often seen in microbeam analyses, especially LA-ICP-MS (Villa *et al.,* 2017). Therefore, it might not reflect geochemical change in samples but simply an analytical error.

In addition to Pb* gain several grains indicated possible low temperature Pb* loss (see green arrows for recent and orange for ancient Pb* loss in Figure 18). Recent Pb* loss might be the result of microbeam analyses similarly to Pb* gain but ancient Pb* loss could be a misinterpretation of growth zones in the grain. If the rim is significantly younger than the core, the received signal can be mixed. (Villa *et al.,* 2017) However, SEM imaging did not reveal apparent growth zones in all of the grains where ancient Pb* loss could be interpreted.

Moreover, there were indications of common lead gain in samples (see blue arrows in Figure 18). These most probably represent non-radiogenic Pb rich inclusions in otherwise Pb-poor zircons (Villa, *et al.,* 2017).

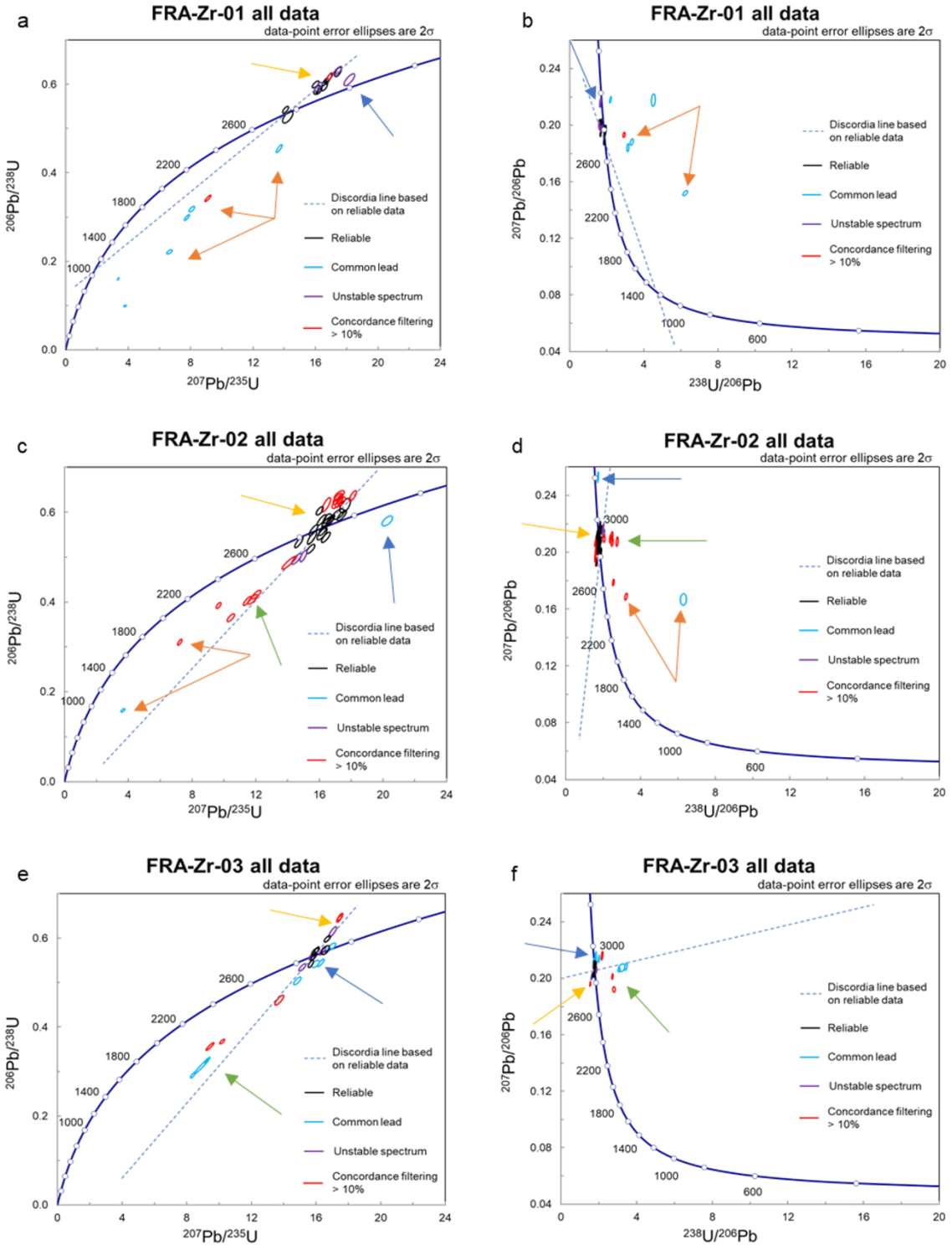

Figure 18. Concordia diagrams for detrital samples with discordia line based on reliable data included. The arrows are colour-coded (see explanation in the text) and indicate different causes for discordance.

The zircons in Doume sample that were separated from a K-bentonite bed showed significantly different morphological appearance and age signal. The zircon grains in DM136 sample were

relatively small and often provided high-intensity ^{204}Pb signal indicating the geochemical resetting of the zircons. On second measuring session two larger grains (Figure 19) DM136-20 and DM136-21 (Appendix 4) in sample DM136, that provided the most reliable signals on first session with 20 µm-diameter beam, were measured with 40 µm laser beam diameter. Both grains revealed zones with high common lead signal. This was not the case on first session, which might be because with smaller spot size different regions were not detected. As a result, only one of the larger grains provided reliable age data using 40 µm laser beam diameter. The final Pb-Pb age yielded for this signal was approximately 2082 Ma (Figure 19b).

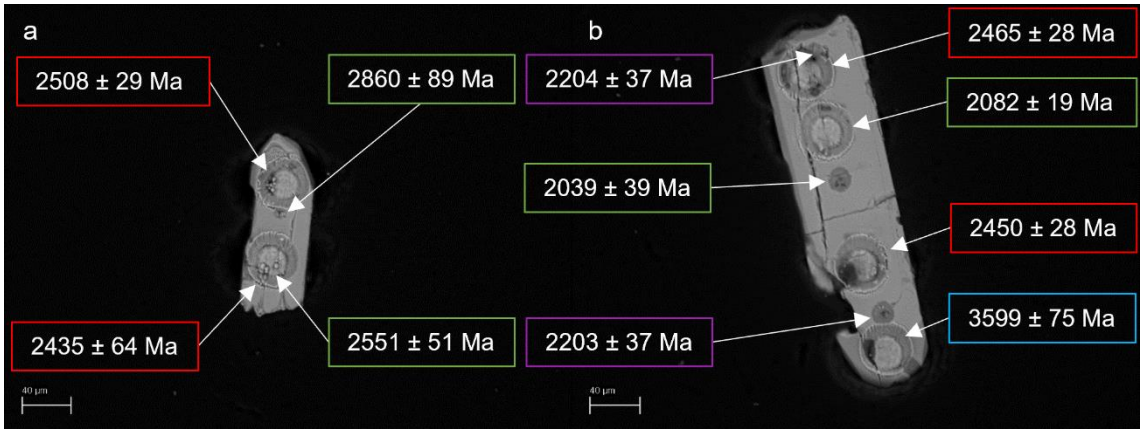

Figure 19. Pb-Pb ages for each measurement in two larger grains in sample DM136. (a) Grain DM136-21. (b) Grain DM136-20. The colour of the box shows the reliability of the data. With green box are reliable data. Blue box displays data with high common lead signal. Purple indicates unstable signal spectrum and red represents concordance filter >20%. The spot that yields age at 3599 ± 75 Ma (b) was lasered through the covering epoxy layer. The most reliable age is from a spot in centre of the zircon at the right (b) showing age 2082 ± 19 Ma.

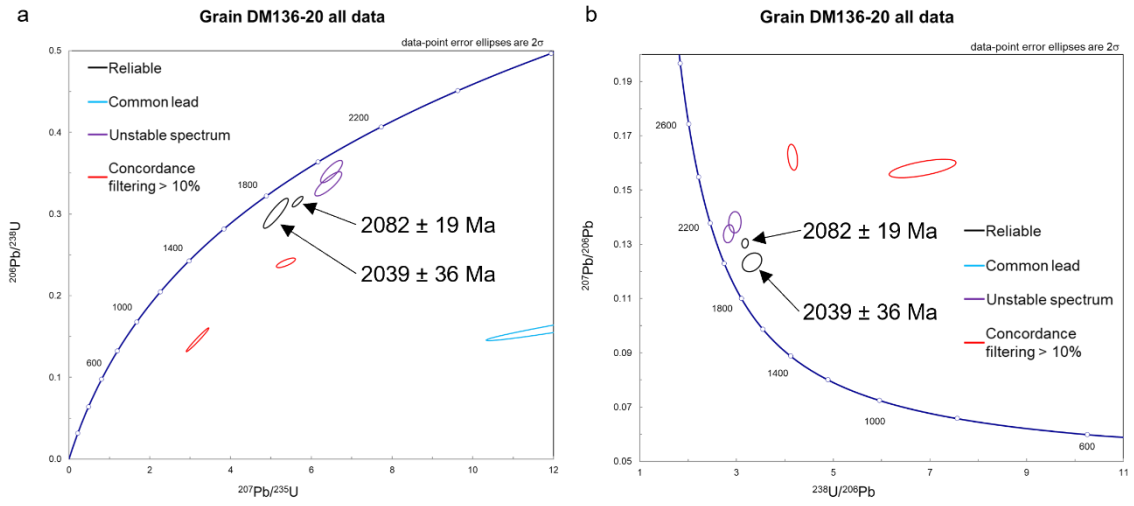

Figure 20. Concordia diagrams for grain DM136-20 that provided the most reliable age for zircons.

The existing understanding of the depositional age of the Francevillian succession is rather poorly constrained between 2500 to 2000 Ma (Weber *et al.*, 2016). The crystalline basement in Francevillian Basin is composed mostly of Meso- to Neoarchaean, in places Paleoproterozoic, crystalline rocks of the Archean Congo Craton (Weber *et al.*, 2016; Thiéblemont *et al.*, 2009) that can be divided into two structural blocks composed of Archean granitoids and greenstone belts, and the Archean and earliest Paleoproterozoic high grade metamorphic terranes intruded with granitoids that were metamorphosed during the ca. 2.2–2.0 Ga Eburnian orogeny (Thiéblemont *et al.*, 2009; Weber et al., 2016; Ossa-Ossa *et al.*, 2020).

The maximum ages of the FA and FB formation deposition in Francevillian Basin are virtually unknown as the minimum ages of the detrital zircons found in FA and FB units scatter between 2703 - 2635 Ma, and 2600 – 2618 Ma, respectively (Ossa-Ossa *et al.*, 2020). The minimum age of the FA and FB formations deposition is constrained by N'goutou granitic intrusion in Okandja sub-basin (Figure 1) that has been dated by U-Pb zircon age at 2191 ± 13 Ma (Sawaki *et al.*, 2017). The zircons derived from an ignimbrite bed in FD formation was dated by U-Pb method at 2083 ± 6 Ma (Horie *et al.*, 2005).

Considering the existing age constraints on the Francevillian sedimentary succession it appears that three samples of the putative pyroclastic beds out of four analysed in this study that were yielding zircon U-Pb ages over 2800 Ma contain only detrital zircon grains. None of the zircon grains in FRA-Zr-01, FRA-Zr-02 and FRA-Zr-03 samples from tuff-like beds in FB2 shales provided reliable Pb-Pb age less than 2776 ± 15 Ma. Zircons are common accessory minerals in felsic to andesitic magmas and therefore it is possible that these beds are not of pyroclastic origin at all as in the case of pyroclastic sediments, zircon grains coeval with sedimentation would have been expected. However, Bankole *et al.* (2018) analysed the zircons derived from a K-bentonite (altered volcanic ash) bed characterized by a typical mixed-layer illite-smectite clay-mineral association and did not found any volcanic zircons. All zircons separated from this bentonite material were detrital with mean Pb-Pb age of 2971 ± 13 Ma (Bankole *et al.*, 2018) that they interpreted as inherited during the magma ascent from the Archean crystalline basement.

On the other hand, ages of the detrital zircons in FB2 formation samples studied here agree well with U-Pb ages of the detrital zircons in FA and FB formations recently studied by Ossa-Ossa *et al*. (2020). They show that the late Mesoarchean zircon population with an age of 2900–2800 Ma is the dominant zircon population in FA and FB sandstones with subordinate

populations (both ca. 20-30% of grains) of middle Mesoarchean zircons with ages 3075–2900 Ma and Neoarchean zircons with 2800–2635 Ma ages. Similar results have been obtained for FA Formation by Mathieu *et al*. (2001) and Bankole *et al.* (2018). Ossa-Ossa *et al*. (2020) interpreted that the Mesoarchean to Neoarchean igneous rocks from the North Gabon and Chaillu massifs were the likely sources for the Francevillian Group sediments deposited in lower part of the succession.

The Doume drillcore K-bentonite revealed a mixed age signal possibly muted by Pb* loss and common-lead contamination. However, one of the largest zircon grains in DM136 sample yielded a nearly concordant Pb-Pb age at 2082 ± 19 Ma. This age agrees within error with the age of the ignimbrite tuff bed in the FD Formation sampled and analysed by Horie *et al.* (2005) that yielded Pb-Pb age of 2083 ± 6 Ma. This age probably represents the depositional age of the FD formation though Weber *et al.* (2016) suggests, by reinterpreting the Horie *et al.* (2005) data that the depositional ages for FD Formation is between 2042 to 2003 Ma. To acquire more reliable age data for FD formation in Francevillian succession more zircon grains from K-bentonites in the formation should be analysed.

Conclusions

The aim of this study was to measure the U-Pb ages of the zircon samples from Francevillian Basin in Gabon using laser-ablation inductively coupled plasma mass-spectrometry (LA-ICP-MS). Reliable age data are necessary for confirming global correlation of these sediments and analysing secular geochemical changes in paleo-environments.

Zircon grains are often used for geological dating because of their durability and naturally high concentrations of U and Th. However, general geological situation and preservation of zircons isotopic signal surrounding the grains is important as well. U-Pb dating of zircons is a valid dating method only if there has been a crystallization (or recrystallization) event where zircons could be formed. Thus, the only sedimentary environments where the age of the formation could be reliably dated by zircons are volcanoclastic sediments or syn-depositional magmatic rocks (i.e., lavas). In other cases, zircons are inherited from surrounding rocks and therefore are of older age.

Three tuff-like samples analysed in this study were from Francevillian FB formation (samples FRA-Zr-01, FRA-Zr-02 and FRA-Zr-03) in Franceville sub-basin and two (DM57 and DM136) from K-bentonites from FD formation in Doume drillcore in Lastrousville sub-basin. The sample DM57 did not contain any measurable zircon grains.

All zircons in three samples from FB formation were of detrital origin with average Pb-Pb ages of more than 2800 Ma. This correlates with the age of the Archean basement in the basin. FD formation K-bentonite sample DM136 from Doume core contained relatively small zircon grains that have possibly experienced changes in isotopic composition in the past, so only one of the analyses of a larger zircon crystal was considered as reliable providing the age of 2082 ± 19 Ma that is consistent with earlier results reported with an ignimbrite bed of the same formation.

However, to confirm these dates and the age of the deposition of the Francevillian succession, further analyses are needed.

Kokkuvõte

Selle töö eesmärk oli dateerida Paleoproterosoilise Franceville'i settebasseini arvatavatest püroklastilistest settekihtidest kogutud tsirkoone U-Pb meetodil laser-ablatsiooni induktiivsidestatud massispektromeetria (LA-ICP-MS) analüüsil. Franceville'i settebasseini täitvate setendite vanus on ligikaudu 2500 kuni 2000 Ma ning nende setendite usaldusväärsed absoluutsed vanusemäärangud on vajalikud, et oleks võimalik kinnitada nende korrelatsioon globaalse kronostratigraafiaga ja nende kasutatavust geokeemiliste trendide iseloomustamiseks.

Tsirkoone kasutatakse tihti geoloogiliste proovide vanuste määramiseks, sest need on vastupidavad väliskeskkonna mõjutustele (keemiline ja füüsikaline murenemine) ja nendes on piisavalt kõrged U-Pb meetodil radioaktiivseks dateerimiseks vajalike uraani ja tooriumi kontsentratsioonid. Sellegipoolest on oluline arvestada ka üldist geoloogilist situatsiooni, sest tsirkoonide abil on võimalik dateerida vaid nende kivimite vanust, mille tekkimise käigus on toimunud tsirkoonide kristalliseerumine või ümberkristalliseerumine. Seetõttu ei ole enamasti võimalik tsirkoonide abil määrata täpselt settekivimite tekkeaega, välja arvatud juhul, kui tegu on püroklastiliste setetega või settimise ajal moodustunud purskekivimitega (nt laavad).

Kolm proovi, mida töös analüüsiti, pärinesid Franceville'i basseini FB kihistust (proovid FRA-Zr-01, FRA-Zr-02 and FRA-Zr-03) Franceville'i alam-basseinis ja kaks proovi (DM57 ja DM136) FD kihistust, mis on avatud Doume puursüdamikus Lastoursville alam-basseinis. Kõigis uuritud proovides välja arvatud proovis DM57 esinesid analüüsitavad tsirkoonid.

Töö tulemusena selgus, et FB kihistu tuffilaadsetest kihtidest pärinevate tsirkoonide keskmised vanused olid üle 2800 Ma. Mõõdetud tsirkoonide vanused on samastatavad basseini Arhaikumi-aegse kristalliinse aluskorra vanusega, seega võib eeldada, et FB kihistu tsirkoonid on detriitsed, st settesse kulutusalalt sisse kantud ning ei näita kihistumise tegelikku aega.

Proovi DM136 tsirkoonid, mis eraldati FD kihistu K-bentoniidist Doume puursüdamikus, olid väga väikesed ja nende kõrged mitte-radiogeense plii sisaldused viitasid terade isotoopse koostise muutusele minevikus. Enamus analüüsitud teradest ei andnud usaldusväärset vanuselist signaali ning sellest proovist saadi vaid ühe suurema tsirkoonitera analüüsimisel usaldusväärne signaal. Selle põhjal määrati tsirkooni Pb-Pb vanuseks 2082 ± 19 Ma, mis vastab hästi varasemalt saadud FD kihistu dateeringutele.

Selleks, et usaldusväärselt dateerida Franceville’i läbilõike erinevaid kihte, on vaja edasisi analüüse uute suuremate proovidega.

Acknowledgements

I would like to thank my supervisors for support and guidance throughout the study and also for the possibility to work on such interesting and internationally important topic.

Appendix 1

Table 1. Analyses from sample FRA-Zr-01.

	ppm										Age (Ma)		Age (Ma)		Age (Ma)	
Grain	Pb	Th	U	U/Th	207Pb/206Pb	2 s. %	207Pb/235U	2 s. %	206Pb/238U	2 s. %	207Pb/206Pb	2 SE	207Pb/235U	2 SE	206Pb/238U	2 SE
FRA-1-01-01	286.5	198.7	549.0	2.80	0.200	0.001	16.600	0.150	0.605	0.007	2827	11	2914	9	3052	29
FRA-1-01-02	132.9	89.3	301.0	3.41	0.199	0.002	16.840	0.180	0.613	0.011	2818	13	2926	10	3081	43
FRA-1-02	151.0	108.8	468.0	4.88	0.181	0.002	8.070	0.140	0.318	0.005	2658	18	2239	16	1780	24
FRA-1-03	80.4	51.4	67.8	1.38	0.215	0.003	18.170	0.280	0.611	0.011	2944	19	2999	15	3088	42
FRA-1-04	93.1	65.6	100.3	1.55	0.197	0.002	16.940	0.170	0.618	0.007	2797	14	2932	10	3109	27
FRA-1-05	198.2	121.7	654.0	5.92	0.187	0.002	7.760	0.130	0.299	0.006	2719	15	2204	16	1687	28
FRA-1-06-01	80.0	51.3	173.3	3.21	0.200	0.002	16.560	0.180	0.596	0.008	2829	14	2910	10	3016	34
FRA-1-06-02	130.0	62.7	273.8	4.29	0.216	0.002	13.680	0.160	0.455	0.007	2950	12	2728	11	2418	33
FRA-1-07	151.7	104.5	165.4	1.60	0.198	0.001	16.230	0.150	0.586	0.007	2807	11	2893	10	2972	27
FRA-1-08	618.0	340.2	857.0	2.94	0.214	0.004	6.640	0.150	0.221	0.004	2956	31	2067	20	1288	22
FRA-1-09	257.8	182.8	259.4	1.45	0.195	0.002	16.020	0.180	0.600	0.006	2787	16	2878	11	3033	25
FRA-1-10	537.0	374.0	457.0	1.24	0.198	0.002	16.090	0.160	0.588	0.008	2812	17	2884	9	2982	33
FRA-1-11	295.8	206.3	445.0	2.17	0.199	0.002	16.190	0.200	0.594	0.008	2817	15	2890	12	3009	33
FRA-1-12	19.3	4.9	189.0	29.70	0.198	0.002	9.110	0.150	0.342	0.006	2812	19	2357	15	1897	29
FRA-1-13	1120.0	1948.0	1315.0	0.69	0.157	0.001	3.356	0.042	0.160	0.003	2426	16	1496	10	958	15
FRA-1-14	651.0	440.0	767.0	1.76	0.194	0.002	14.090	0.150	0.543	0.006	2776	15	2756	10	2796	27
FRA-1-15	97.9	68.2	193.3	2.77	0.205	0.003	17.440	0.180	0.628	0.009	2869	19	2960	10	3142	35
FRA-1-16	405.0	283.0	207.0	0.70	0.205	0.002	17.430	0.210	0.631	0.008	2868	17	2959	11	3152	31
FRA-1-17	638.0	930.0	923.0	0.93	0.283	0.006	3.803	0.060	0.099	0.002	3379	29	1596	13	609	11
FRA-1-18	61.0	87.1	155.0	1.68	0.198	0.002	14.230	0.270	0.526	0.011	2808	15	2767	18	2730	48

Appendix 2

Table 2. Analyses from sample FRA-Zr-02.

Grain	ppm Pb	Th	U	U/Th	207Pb/206Pb	2 s. %	207Pb/235U	2 s. %	206Pb/238U	2 s. %	Age (Ma) 207Pb/206Pb	2 SE	Age (Ma) 207Pb/235U	2 SE	Age (Ma) 206Pb/238U	2 SE
FRA-2-01	121.9	103.2	260.2	2.52	0.210	0.003	17.630	0.270	0.615	0.013	2905	18	2974	15	3091	52
FRA-2-02	264.1	174.6	463.0	2.57	0.195	0.003	16.430	0.220	0.617	0.013	2790	21	2903	13	3101	49
FRA-2-03	16.3	26.7	40.6	1.52	0.211	0.003	10.440	0.200	0.365	0.007	2912	23	2477	17	2007	32
FRA-2-04	44.8	23.7	373.0	15.37	0.202	0.002	14.720	0.210	0.533	0.010	2845	14	2798	14	2754	41
FRA-2-05	135.2	102.1	318.2	2.98	0.195	0.002	16.010	0.180	0.603	0.007	2784	19	2881	10	3042	30
FRA-2-06	36.2	27.3	33.1	1.19	0.208	0.003	17.190	0.310	0.596	0.010	2890	24	2951	17	3013	39
FRA-2-07	222.3	155.8	386.0	2.41	0.198	0.002	17.270	0.170	0.629	0.009	2815	18	2951	10	3148	36
FRA-2-08-01	207.6	142.1	288.4	1.95	0.199	0.002	17.330	0.270	0.622	0.009	2822	19	2961	14	3119	36
FRA-2-08-02	336.0	252.1	162.5	0.65	0.196	0.003	17.140	0.290	0.622	0.011	2795	20	2943	17	3126	45
FRA-2-09	220.4	159.9	337.9	2.05	0.193	0.002	17.250	0.250	0.638	0.008	2768	19	2950	14	3188	31
FRA-2-10	177.0	129.7	324.3	2.35	0.202	0.002	16.490	0.200	0.586	0.009	2846	14	2908	12	2973	35
FRA-2-11	223.0	154.4	213.5	1.32	0.189	0.002	17.130	0.240	0.630	0.010	2735	17	2943	14	3159	43
FRA-2-12	733.0	68.3	556.0	8.04	0.247	0.004	20.260	0.270	0.581	0.009	3163	25	3107	13	2962	36
FRA-2-13	61700.0	51450.0	442.0	0.01	0.200	0.003	15.530	0.240	0.543	0.012	2826	21	2853	15	2797	51
FRA-2-14	339.0	358.2	741.0	2.02	0.175	0.002	9.670	0.130	0.393	0.006	2606	19	2405	12	2134	26
FRA-2-15	97.4	67.2	214.7	3.13	0.203	0.002	18.110	0.190	0.636	0.010	2846	17	2997	10	3175	40
FRA-2-16	193.0	135.5	311.6	2.28	0.198	0.002	16.470	0.250	0.578	0.009	2808	17	2906	14	2945	37
FRA-2-17	245.4	162.5	577.0	3.52	0.199	0.002	16.680	0.190	0.582	0.009	2817	17	2918	12	2958	36
FRA-2-18	197.2	136.6	170.2	1.19	0.201	0.002	17.420	0.240	0.593	0.010	2836	19	2961	13	3003	38
FRA-2-19	302.0	209.5	369.0	1.80	0.197	0.002	16.720	0.190	0.584	0.009	2804	15	2920	11	2967	36
FRA-2-20	72.6	53.8	158.8	2.84	0.210	0.002	16.410	0.220	0.544	0.010	2903	13	2904	13	2801	40
FRA-2-21	101.9	81.7	136.4	1.64	0.205	0.002	15.450	0.210	0.519	0.008	2869	16	2845	13	2695	35
FRA-2-22	77.5	74.5	296.9	3.96	0.201	0.002	12.040	0.240	0.417	0.008	2833	17	2608	19	2252	37
FRA-2-23	582.0	335.0	1098.0	3.62	0.154	0.003	3.650	0.100	0.159	0.003	2393	39	1565	21	950	18
FRA-2-24	45.2	43.6	81.9	1.80	0.204	0.003	15.000	0.180	0.503	0.011	2861	24	2818	11	2625	46
FRA-2-25	173.1	119.5	290.7	2.44	0.203	0.003	16.180	0.260	0.552	0.011	2852	20	2891	15	2840	44
FRA-2-26-01	142.7	70.7	357.8	5.63	0.201	0.003	11.810	0.250	0.406	0.009	2833	23	2589	20	2197	41
FRA-2-26-02	76.3	56.6	93.3	1.61	0.208	0.003	14.570	0.250	0.496	0.010	2892	23	2793	17	2607	43
FRA-2-27	292.9	381.0	736.0	1.96	0.165	0.002	7.230	0.110	0.311	0.006	2506	16	2141	14	1744	27
FRA-2-28-01	145.5	90.6	215.0	2.38	0.200	0.003	16.200	0.190	0.559	0.009	2830	21	2890	11	2866	37
FRA-2-28-02	307.1	221.0	331.2	1.53	0.197	0.002	16.140	0.240	0.583	0.010	2802	16	2889	14	2959	41
FRA-2-29-01	116.3	34.9	294.6	9.34	0.200	0.003	11.480	0.200	0.402	0.008	2826	21	2565	16	2184	40
FRA-2-29-02	76.8	13.6	364.6	21.50	0.204	0.003	14.110	0.370	0.488	0.012	2857	22	2770	25	2571	57
FRA-2-30	152.7	99.8	293.4	2.96	0.199	0.002	15.640	0.220	0.561	0.010	2825	19	2855	14	2869	40

Appendix 3.

Table 3. Analyses from sample FRA-Zr-03.

	ppm										Age (Ma)		Age (Ma)		Age (Ma)	
Grain	Pb	Th	U	U/Th	207Pb/206Pb	2 s. %	207Pb/235U	2 s. %	206Pb/238U	2 s. %	207Pb/206Pb	2 SE	207Pb/235U	2 SE	206Pb/238U	2 SE
FRA-3-01-01	276.5	181.4	412.1	2.28	0.197	0.001	17.470	0.140	0.646	0.005	2800	11	2962	8	3211	20
FRA-3-01-02	283.6	182.9	421.9	2.26	0.201	0.002	17.030	0.200	0.615	0.010	2834	12	2936	11	3090	39
FRA-3-02	233.8	150.7	437.8	2.89	0.196	0.002	17.470	0.150	0.646	0.008	2795	13	2964	8	3213	32
FRA-3-03	206.6	90.1	446.0	4.72	0.206	0.002	9.260	0.140	0.326	0.005	2873	13	2363	14	1818	25
FRA-3-04	194.8	149.7	169.3	1.10	0.214	0.002	14.840	0.190	0.504	0.007	2931	15	2806	11	2627	31
FRA-3-05-01	401.0	729.0	461.0	0.62	0.207	0.002	8.380	0.130	0.292	0.005	2882	14	2273	14	1649	25
FRA-3-05-02	63.9	48.6	67.5	1.38	0.213	0.003	15.970	0.180	0.542	0.007	2927	20	2874	11	2794	30
FRA-3-06	56.1	45.2	126.1	2.71	0.211	0.002	16.970	0.200	0.581	0.007	2916	15	2931	11	2955	26
FRA-3-07-01	36.2	88.5	150.0	1.59	0.209	0.002	8.930	0.380	0.312	0.014	2894	18	2316	38	1741	66
FRA-3-07-02	47.7	39.3	258.4	6.52	0.207	0.002	16.410	0.170	0.572	0.008	2882	12	2904	10	2916	32
FRA-3-08	103.7	80.6	101.9	1.25	0.206	0.002	15.800	0.190	0.560	0.007	2875	17	2866	12	2864	30
FRA-3-09	45.2	74.0	108.4	1.48	0.217	0.003	13.730	0.220	0.461	0.009	2951	19	2730	16	2445	40
FRA-3-10	167.6	108.4	471.7	4.43	0.218	0.001	16.300	0.170	0.544	0.007	2966	10	2893	10	2800	29
FRA-3-11	149.5	112.2	242.8	2.17	0.205	0.002	15.860	0.150	0.559	0.007	2868	13	2868	9	2862	27
FRA-3-12	53.9	56.6	541.6	9.78	0.195	0.002	9.440	0.210	0.357	0.007	2782	13	2383	21	1967	33
FRA-3-13	105.5	74.4	147.3	2.00	0.203	0.002	15.940	0.170	0.570	0.006	2850	15	2873	10	2908	25
FRA-3-14	97.1	86.0	226.6	2.63	0.204	0.001	16.700	0.160	0.598	0.006	2855	11	2917	9	3022	25
FRA-3-15	83.1	58.2	256.6	4.35	0.201	0.002	10.200	0.120	0.368	0.005	2836	13	2451	11	2017	22
FRA-3-16	155.8	129.8	161.1	1.26	0.206	0.002	15.150	0.180	0.534	0.007	2873	14	2826	11	2757	28
FRA-3-17	161.8	127.5	294.1	2.30	0.205	0.002	16.050	0.120	0.573	0.006	2863	12	2880	7	2922	24
FRA-3-18-01	109.3	78.9	220.6	2.78	0.211	0.002	15.680	0.140	0.542	0.007	2909	14	2857	9	2797	29
FRA-3-18-02	86.6	59.3	93.1	1.57	0.214	0.002	16.580	0.200	0.573	0.008	2933	17	2912	12	2919	34

Appendix 4

Table 4. Analyses from sample DM136.

Grain	ppm Pb	Th	U	U/Th	207Pb/206Pb	2 s. %	207Pb/235U	2 s. %	206Pb/238U	2 s. %	Age (Ma) 207Pb/206Pb	2 SE	Age (Ma) 207Pb/235U	2 SE	Age (Ma) 206Pb/238U	2 SE
DM136-01-01	244.0	294.0	316.0	1.07	0.148	0.003	6.250	0.140	0.306	0.010	2330	38	19	1719	47	1590
DM136-01-02	264.0	368.0	452.0	1.23	0.137	0.003	4.280	0.140	0.226	0.009	2187	32	29	1308	45	1330
DM136-02-01	234.0	316.0	476.0	1.51	0.136	0.003	5.580	0.150	0.301	0.008	2168	37	22	1695	38	1470
DM136-02-02	6100.0	614.0	1230.0	2.00	0.509	0.031	49.000	16.000	0.490	0.130	4233	88	230	2090	400	14100
DM136-03-01	409.0	493.0	593.0	1.20	0.153	0.003	5.220	0.130	0.243	0.007	2389	36	21	1401	35	1700
DM136-03-02	650.0	407.0	488.0	1.20	0.241	0.008	8.310	0.290	0.250	0.006	3124	58	33	1439	33	3090
DM136-04	1150.0	1480.0	2020.0	1.36	0.306	0.024	3.020	0.560	0.074	0.008	3390	110	64	455	45	1510
DM136-05	325.0	709.0	930.0	1.31	0.157	0.008	1.990	0.130	0.097	0.005	2377	72	40	595	31	1011
DM136-06	28200.0	5110.0	5540.0	1.08	0.696	0.040	25.000	5.400	0.228	0.044	4730	100	240	1240	210	8000
DM136-07	364.0	455.0	607.0	1.33	0.159	0.004	4.860	0.140	0.222	0.007	2455	39	24	1291	36	1760
DM136-09	383.0	720.0	730.0	1.01	0.146	0.005	3.670	0.270	0.181	0.012	2289	56	63	1063	63	1560
DM136-10	279.0	440.0	367.0	0.83	0.139	0.003	6.120	0.180	0.328	0.012	2216	39	25	1820	59	1790
DM136-11	473.0	1350.0	1290.0	0.96	0.161	0.004	2.340	0.110	0.109	0.004	2458	43	35	671	25	1100
DM136-12-01	536.0	261.0	242.0	0.93	0.457	0.031	13.040	0.810	0.227	0.009	3980	120	61	1318	49	6350
DM136-12-02	404.0	594.0	547.0	0.92	0.154	0.003	6.000	0.140	0.291	0.008	2390	32	20	1645	40	1890
DM136-13	517.0	709.0	543.0	0.77	0.145	0.003	5.820	0.180	0.303	0.013	2286	32	27	1699	62	1950
DM136-14-01	484.0	1146.0	1010.0	0.88	0.197	0.006	2.530	0.110	0.092	0.003	2783	48	30	564	16	-302
DM136-14-02	226.0	270.0	330.0	1.22	0.153	0.004	5.460	0.220	0.273	0.012	2376	41	34	1549	59	2250
DM136-15-01	262.0	242.0	335.0	1.38	0.178	0.005	5.860	0.210	0.249	0.009	2626	50	30	1429	45	2860
DM136-15-02	355.0	446.0	363.0	0.81	0.155	0.004	6.610	0.230	0.332	0.011	2394	44	31	1842	52	2040
DM136-16	242.0	294.0	284.0	0.97	0.148	0.005	6.570	0.180	0.337	0.012	2303	51	24	1863	58	2050
DM136-17-01	572.0	618.0	766.0	1.24	0.192	0.004	4.520	0.160	0.183	0.007	2747	34	28	1083	38	2198
DM136-17-02	565.0	530.0	690.0	1.30	0.263	0.021	4.850	0.190	0.157	0.010	3205	92	33	940	52	1990
DM136-18	383.0	373.0	478.0	1.28	0.197	0.007	3.600	0.110	0.133	0.006	2777	54	25	802	36	-343
DM136-19	199.0	233.0	235.5	1.01	0.144	0.004	5.670	0.150	0.305	0.009	2266	45	23	1711	45	1700
DM136-20-01	3430.0	319.0	554.0	1.74	0.492	0.028	31.700	3.500	0.451	0.036	4212	85	110	2370	160	13310
DM136-20-02	179.0	211.0	265.0	1.26	0.137	0.003	6.500	0.220	0.352	0.011	2203	37	29	1943	53	1690
DM136-20-03	133.0	149.0	285.7	1.92	0.127	0.003	5.120	0.250	0.301	0.015	2039	36	40	1692	75	1850
DM136-20-04	184.0	173.0	294.0	1.70	0.138	0.003	6.420	0.270	0.337	0.012	2204	37	37	1870	57	2370
DM136-20-05	1140.0	219.1	388.8	1.76	0.337	0.019	12.900	2.100	0.167	0.018	3599	75	2500	110	976	92

DM136-20-06	184.0	172.3	319.0	1.84	0.160	0.003	5.370	0.190	0.240	0.005	2450	28	1871	30	1387	25
DM136-20-07	106.2	113.9	237.2	1.99	0.129	0.001	5.660	0.110	0.315	0.005	2082	19	1922	16	1764	26
DM136-21-01	144.2	196.5	431.0	2.10	0.161	0.003	3.180	0.230	0.146	0.012	2465	28	1438	53	871	64
DM136-21-02	382.0	415.1	334.9	0.78	0.161	0.006	7.560	0.250	0.345	0.006	2435	64	2170	28	1910	28
DM136-21-03	403.2	397.0	368.0	0.90	0.165	0.003	7.400	0.220	0.323	0.004	2508	29	2152	26	1802	22
DM136-21-04	195.0	123.8	170.0	1.37	0.168	0.005	9.190	0.400	0.395	0.015	2551	51	41	2169	69	3400
DM136-21-05	356.0	123.3	180.0	1.46	0.211	0.012	13.630	0.940	0.477	0.015	2860	89	63	2512	68	5500
DM136-22-01	301.0	870.0	980.0	1.13	0.126	0.004	2.860	0.220	0.167	0.013	2029	52	67	993	72	1140
DM136-22-02	1190.0	980.0	1140.0	1.16	0.208	0.019	4.880	0.540	0.176	0.012	2700	110	72	1033	68	2220
DM136-23-01	371.0	292.0	595.0	2.04	0.154	0.003	6.300	0.310	0.298	0.016	2389	36	43	1684	77	2680
DM136-23-02	430.0	332.0	638.0	1.92	0.166	0.004	6.140	0.220	0.269	0.013	2519	42	32	1535	66	2660

References

Ausmeel, M., 2020. Lewisian'i gneisikompleksi tsirkooni megakristallide sobivusehindamine in-house U - Pb dateerimise standardina LA-ICP-MS meetodil Tartu University, Tartu, 44 pp.

Bankole, O.M., El Albani, A., Meunier, A., Pambo, F., Paquette, J.L. and Bekker, A., 2018. Earth's Oldest Preserved K-Bentonites in the Ca. 2.1 Ga Francevillian Basin, Gabon. American Journal of Science, 318(4): 409-434.

Bankole, O.M., El Albani, A., Meunier, A., Rouxel, O.J., Gauthier-Lafaye, F. and Bekker, A., 2016. Origin of Red Beds in the Paleoproterozoic Franceville Basin, Gabon, and Implications for Sandstone-Hosted Uranium Mineralization. American Journal of Science, 316(9): 839-872.

Blättler, C.L., Claire, M.W., Prave, A.R., Kirsimäe, K., Higgins, J.A., Medvedev, P.V., Romashkin, A.E., Rychanchik, D.V., Zerkle, A.L., Paiste, K., Kreitsmann, T., Millar, I.L., Hayles, J.A., Bao, H., Turchyn, A.V., Warke, M.R. and Lepland, A., 2018. Two-billion-year-old evaporites capture Earth's great oxidation. Science, 360(6386): 320-323.

Bros, R., Stille, P., Gauthierlafaye, F., Weber, F. and Clauer, N., 1992. Sm-Nd Isotopic Dating of Proterozoic Clay Material - an Example from the Francevillian Sedimentary Series, Gabon. Earth and Planetary Science Letters, 113(1-2): 207-218.

El Albani, A., Bengtson, S., Canfield, D.E., Bekker, A., Macchiarelli, R., Mazurier, A., Hammarlund, E.U., Boulvais, P., Dupuy, J.J., Fontaine, C., Fursich, F.T., Gauthier-Lafaye, F., Janvier, P., Javaux, E., Ossa, F.O., Pierson-Wickmann, A.C., Riboulleau, A., Sardini, P., Vachard, D., Whitehouse, M. and Meunier, A., 2010. Large colonial organisms with coordinated growth in oxygenated environments 2.1 Gyr ago. Nature, 466(7302): 100-104.

Farquhar, J., Bao, H.M. and Thiemens, M., 2000. Atmospheric influence of Earth's earliest sulfur cycle. Science, 289(5480): 756-758.

Gauthierlafaye, F. and Weber, F., 1989. The Francevillian (Lower Proterozoic) Uranium Ore-Deposits of Gabon. Economic Geology, 84(8): 2267-2285.

Griffin, B.J., 2000. Charge contrast imaging of material growth and defects in environmental scanning electron miscroscopy - Linking electron emission and cathodoluminescence. Scanning, 22(4): 234-242.

Gumsley, A.P., Chamberlain, K.R., Bleeker, W., Soderlund, U., Kock, M.D.O., Larsson, E.R. and Bekker, A., 2017. Timing and tempo of the Great Oxidation Event. Proceedings of the National Academy of Sciences of the United States of America, 114(8): 1811-1816.

Holland, H.D., 2006. The oxygenation of the atmosphere and oceans. Philosophical Transactions of the Royal Society B-Biological Sciences, 361(1470): 903-915.

Horie, K., Hidaka, H. and Gauthier-LaFaye, F., 2005. U-Pb geochronology and geochemistry of zircon from the Franceville series at Bidoudouma, Gabon. Geochimica et Cosmochimica Acta, 69(10): A11-A11.

Karhu, J.A. and Holland, H.D., 1996. Carbon isotopes and the rise of atmospheric oxygen. Geology, 24(10): 867-870.

Kosler, J., 2007. Laser ablation ICP-MS - a new dating tool in Earth science. Proceedings of the Geologists Association, 118: 19-24.

Lepland, A., Melezhik, V.A., Papineau, A.E., Romashkin, A.E. and Joosu, L., 2013. The Earliest Phosphorites – Radical Change in the Phosphorus Cycle during the Palaeoproterozoic. In: V.A. Melezhik, A.R. Prave, A.E. Fallick, L.R. Kump, H.

Strauss, A. Lepland and E. Hanski (Editors), Reading the Archive of Earth's Oxygenation: Volume 3: Global Events and the Fennoscandian Arctic Russia - Drilling Early Earth Project. Frontiers in Earth Sciences. Springer, pp. 1275-1296.
Longerich, H.P., 2008. Laser Ablation-Inductively Coupled Plasma-Mass Spectrometry: An Introduction. In: P. Sylvester (Editor), Laser-Ablation-ICP-MS in the Earth Sciences: Current Practices and Outstanding Issues. Mineralogical Association of Canada, pp. 1-18.
Luo, G.M., Ono, S.H., Beukes, N.J., Wang, D.T., Xie, S.C. and Summons, R.E., 2016. Rapid oxygenation of Earth's atmosphere 2.33 billion years ago. Science Advances, 2(5).
Lyons, T.W., Reinhard, C.T. and Planavsky, N.J., 2014. The rise of oxygen in Earth's early ocean and atmosphere. Nature, 506(7488): 307-315.
Martin, A.P., Condon, D.J., Prave, A.R. and Lepland, A., 2013. A review of temporal constraints for the Palaeoproterozoic large, positive carbonate carbon isotope excursion (the Lomagundi-Jatuli Event). Earth-Science Reviews, 127: 242-261.
Mayika, K.B., Moussavou, M., Prave, A.R., Lepland, A., Mbina, M. and Kirsimae, K., 2020. The Paleoproterozoic Francevillian succession of Gabon and the Lomagundi-Jatuli event. Geology, 48(11): 1099-1104.
Melezhik, V.A., Fallick, A.E., Filippov, M.M., Deines, Y.E., Črne, A.E., Lepland, A., Brasier, A.T. and Strauss, H., 2012. Giant Palaeoproterozoic Petrified Oil Field in the Onega Basin. In: V.A. Melezhik, A.R. Prave, A.E. Fallick, L.R. Kump, H. Strauss, A. Lepland and E.J. Hanski (Editors), Reading the Archive of Earth's Oxygenation: Volume 3: Global Events and the Fennoscandian Arctic Russia - Drilling Early Earth Project. Frontiers in Earth Sciences. Springer, pp. 1202-1212.
Melezhik, V.A., Medvedev, P.V. and Svetov, S.A., 2013. The Onega Basin. In: V.A. Melezhik, A.R. Prave, E.J. Hanski, A.E. Fallick, A. Lepland, L.R. Kump and H. Strauss (Editors), Reading the Archive of Earth's Oxygenation: Volume 1: The Paleoproterozoic of Fennoscandia as Context for the Fennoscandian Arctic Russia - Drilling Early Earth Project. Frontiers in Earth Sciences. Springer, pp. 249-287.
Mouele, I.M., Dudoignon, P., El Albani, A., Meunier, A., Boulvais, P., Gauthier-Lafaye, F., Paquette, J.L., Martin, H. and Cuney, M., 2014. 2.9-1.9 Ga paleoalterations of Archean granitic basement of the Franceville basin (Gabon). Journal of African Earth Sciences, 97: 244-260.
Moussavou, M. and Edou Minko, A., 2006. Contribution a` l'histoire thermotectonique pre´cambrienne du complexe annulaire de N'goutou par la ge´ochimie et la ge´ochronologie U/Pb sur mine´raux accessoires (Bassin Francevillien d'Okondja, Gabon). Africa Geoscience Review, 13(1): 53–62.
Ossa, F., Hofmann, A., Wille, M., Spangenberg, J.E., Bekker, A., Poulton, S.W., Eickmann, B. and Schoenberg, R., 2018. Aerobic iron and manganese cycling in a redox-stratified Mesoarchean epicontinental sea. Earth and Planetary Science Letters, 500: 28-40.
Ossa, F.O., El Albani, A., Hofmann, A., Bekker, A., Gauthier-Lafaye, F., Pambo, F., Meunier, A., Fontaine, C., Boulvais, P., Pierson-Wickmann, A.C., Cavalazzi, B. and Macchiarelli, R., 2013. Exceptional preservation of expandable clay minerals in the ca. 2.1 Ga black shales of the Francevillian basin, Gabon and its implication for atmospheric oxygen accumulation. Chemical Geology, 362: 181-192.
Ossa, F.O., Hofmann, A., Ballouard, C., Vorster, C., Schoenberg, R., Fiedrich, A., Mayaga-Mikolo, F. and Bekker, A., 2020. Constraining provenance for the uraniferous Paleoproterozoic Francevillian Group sediments (Gabon) with detrital zircon geochronology and geochemistry. Precambrian Research, 343.

Poulton, S.W., Bekker, A., Cumming, V.M., Zerkle, A.L., Canfield, D.E. and Johnston, D.T., 2021. A 200-million-year delay in permanent atmospheric oxygenation. Nature, 592(7853): 232-+.
Preat, A., Bouton, P., Thieblemont, D., Prian, J.P., Ndounze, S.S. and Delpomdor, F., 2011. Paleoproterozoic high delta C-13 dolomites from the Lastoursville and Franceville basins (SE Gabon): Stratigraphic and synsedimentary subsidence implications. Precambrian Research, 189(1-2): 212-228.
Sawaki, Y., Moussavou, M., Sato, T., Suzuki, K., Ligna, C., Asanuma, H., Sakata, S., Obayashi, H., Hirata, T. and Edou-Minko, A., 2017. Chronological constraints on the Paleoproterozoic Francevillian Group in Gabon. Geoscience Frontiers, 8(2): 397-407.
Spencer, C.J., Kirkland, C.L. and Taylor, R.J.M., 2016. Strategies towards statistically robust interpretations of in situ U-Pb zircon geochronology. Geoscience Frontiers, 7(4): 581-589.
Stille, P., Gauthierlafaye, F. and Bros, R., 1993. The Neodymium Isotope System as a Tool for Petroleum-Exploration. Geochimica Et Cosmochimica Acta, 57(18): 4521-4525.
Thiéblemont, P., Castaing, C., Billa, M., Bouton, P. and Préat, A., 2009. Notice explicative de la carte géologique et des ressources minérales de la République Gabonaise à 1/1000 000: Libreville, Gabon, Ministère des Mines, du Pétrole, des Hydrocarbures, Libreville.
Watt, G.R., Griffin, B.J. and Kinny, P.D., 2000. Charge contrast imaging of geological materials in the environmental scanning electron microscope. American Mineralogist, 85(11-12): 1784-1794.
Weber, F., 1968. Une série précambrienne du Gabon: le Francevillien Sédimentologie, géochimie, relations avec les gîtes minéraux associés. CEA-R-40055, Université de Strasbourg, Strasbourg.
Weber, F. and Gauthier-Lafaye, F., 2013. No proof from carbon isotopes in the Francevillian (Gabon) and Onega (Fennoscandian shield) basins of a global oxidation event at 1980-2090 Ma following the Great Oxidation Event (GOE). Comptes Rendus Geoscience, 345(1): 28-35.
Weber, F., Gauthier-Lafaye, F., Whitechurch, H., Ulrich, M. and El Albani, A., 2016. The 2-Ga Eburnean Orogeny in Gabon and the opening of the Francevillian intracratonic basins: A review. Comptes Rendus Geoscience, 348(8): 572-586.
Vermeesch, P., 2017. Radiometric Geochronology, Isotope Geology. https://eartharxiv.org/.
White, W.M., 2015. Geochemistry. Wiley-Blackwell, Chichester.
Villa, I.M. and Hanchar, J.M., 2017. Age discordance and mineralogy. American Mineralogist, 102(12): 2422-2439.
Wilschefski, S.C. and Baxter, M.R., 2019. Inductively Coupled Plasma Mass Spectrometry: Introduction to Analytical Aspects. The Clinical biochemist. Reviews, 40(3): 115-133.
Üpraus, K., 2014. Chert-dolostone sequences in Zaonega Formation, Karelia: implication to the chert origin, Tartu University, Tartu, 50 pp.

Lihtlitsents lõputöö reprodutseerimiseks ja üldsusele kättesaadavaks tegemiseks

Mina, Carmel Kuusk,

1. annan Tartu Ülikoolile tasuta loa (lihtlitsentsi) minu loodud teose

Dating zircons from Francevillian Basin by laser-ablation inductively coupled plasma mass-spectrometry,

mille juhendajad on Kalle Kirsimäe, Päärn Paiste,

reprodutseerimiseks eesmärgiga seda säilitada, sealhulgas lisada digitaalarhiivi DSpace kuni autoriõiguse kehtivuse lõppemiseni.

2. Annan Tartu Ülikoolile loa teha punktis 1 nimetatud teos üldsusele kättesaadavaks Tartu Ülikooli veebikeskkonna, sealhulgas digitaalarhiivi DSpace kaudu Creative Commonsi litsentsiga CC BY NC ND 3.0, mis lubab autorile viidates teost reprodutseerida, levitada ja üldsusele suunata ning keelab luua tuletatud teost ja kasutada teost ärieesmärgil, alates ***01.06.2023*** kuni autoriõiguse kehtivuse lõppemiseni.

3. Olen teadlik, et punktides 1 ja 2 nimetatud õigused jäävad alles ka autorile.

4. Kinnitan, et lihtlitsentsi andmisega ei riku ma teiste isikute intellektuaalomandi ega isikuandmete kaitse õigusaktidest tulenevaid õigusi.

Carmel Kuusk

01.06.2021